FACULTY OF SCIENCE AND TECHNOLOGY

BACHELOR'S THESIS

Study programme / specialisation: Mechanical engineering	The *autumn* semester, *2022* Open / Confidential
Author: Stian Egseth	
Supervisor at UiS: Vidar Hansen Co-supervisor: External supervisor(s):	
Thesis title: Mechanical properties and microstructure of 17-4 Ph stainless steel made by Jet binder additive manufacturing	
Credits (20):	
Keywords: Additive manufacturing 3D printing 17-4 PH Mechanical properties Microstructure	Pages: + appendix: Stavanger, *31.12.2022*

Abstract

Additive manufacturing is a field seeing constant innovation. This thesis looks at the mechanical properties and microstructure of a Binder Jet Printing (BJP) technology using the stainless steel alloy 17-4 PH. 17-4 PH is a precipitation hardenable steel. Specimen have been tested in the As-printed, H900 and H1150 condition. Hardness, Charpy V-notch CVN and Tensile testing were performed on the sample. The microstructure was studied using light optical microscope LOM and scanning electron microscope SEM. The fractured surface after CVN and tensile testing were studied using SEM. Hardness testing was performed inn the three axes, and seemed to suggest that the material is isotropic. The as- sintered microstructure was heavily influenced by the sintering process. Large particles were seen, particularly adjacent to pores and at grain boundaries. They are though to be detrimental to the mechanical properties as suggested by the fractography. The H1150 was the most ductile of all the conditions, it also displayed the highest CVN-toughness and low strainrate toughness. H900 showed the greatest ultimate strength and had slightly longer elongation than the as-printed, but showed very low CVN resistance. It was concluded that longer solution treatment might result in better mechanical properties, as it reduces the amount of retained δ-ferrite and dissolves the large particles.

Acknowledgement

First of all, I would like to thank Professor Vidar Hansen who has been my faculty supervisor during this thesis for giving me the opportunity of doing this study.

Then I would like to sincerely thank Gabriele Impellizzeri at AIDRO for supplying the material and making the study possible. I also want to show gratitude towards the University of Stavanger for enabling the research by providing the equipment.

A lot of people were involved in the thesis, without them the thesis would not be possible

Wakshum Mekonnen Tucho for kindly helping us with SEM.

Johan Andreas Håland Thorkaas for teaching us how to use the laboratory equipment and for his dedicated assistance with the tensile testing.

Emil Mannes Surnevik at UiS, helped machine the parts.

Marius Belsvik at Kverneland Group AS for his valuable advice and for providing a means to perform heat treatments.

Erling Monsen at UiS for assistance in etching and chemistry.

Jåttå Gårdsbryggeri AS and Diesel & Komponent service AS for allowing me to work in to their workshop and laboratory facilities.

Mats Ingdal for training in the chemistry lab.

And to my employer Kalle & Kjetils rør AS for allowing me the flexible hours, making the thesis work possible.

Martin for valuable assistance and friendship.

Abbreviations

SEM	Scanning electron microscope
LOM	Light optical microscope
AP	As printed
BSE	Back scatter electron
MVC	Micro void coalescence
EDS	Energy dispersive spectroscopy
XRD	X-ray diffraction
SE	Secondary electrons
HV	Hardness Vickers
BJP	Binder Jet Printing
PH	Precipitation hardenable
BCC	Body-centered cubic
FCC	Face-centered cubic
BCT	Body-centered tetragonal
PIM	Powder injection moulding
MIM	Metal injection moulding
CVN	Charpy V-notch
ASM	American society for metals
ASTM	American society for testing and materials
MPIF	Metal powder industries federation
CAD	Computer-aided design
CNC	Computer numerical control
δ	Delta
γ	Gamma
α	Alpha

Index

1 Introduction

Additive manufacturing has been given attention in the last several years. A lot attention has been devoted to technologies that rely on melting the powder to obtain cohesion. This has its downsides, control of the final microstructure can be difficult and the material often ends up with a anisotropic microstructure. Meaning that the mechanical properties can vary in relation to the build direction. JBP is a technology that has its roots form the 1980's. The main principle is that the part geometry is built incrementally in a build bed by fusing cross sections together using a binding agent. When the printing is completed, the part is cured. This gives it the strength to withstand mechanical cleaning of residual powder. The part can now be sintered in a furnace capable of high temperatures and partial atmospheres. Sintering is a process where the powered particles fuse together by diffusion. A regime of temperature and time is followed to achieve the densest product possible. The act of holding a part at an elevated temperature where the goal is to eliminate voids and pores through diffusion is called densification. Densification can be manipulated in several other ways than temperature, the atmosphere is also important. The sintering process results in an isotropic structure that should display the same mechanical properties in any direction.

17-4 PH is a precipitation hardenable stainless steel, this alloy is popular in the AM industry, and has been utilized in several different technologies. The alloy is weldable and shows good corrosion properties. A range of mechanical properties can be achieved by heat treatment. The mechanism is copper in solid solution. Martensite can achieve supersaturation of copper through solution treatment subsequent aging leads to precipitation of copper particles as the martensite tempers. Over aging, is aging beyond the point were peak hardness is achieved, the copper particles become large and loose coherency with the matrix. Diffusion of copper can lead to the formation of austenite in the lath boundaries of the martensite.

The Shop system, by Desktop metal, is a system that utilizes JBP technology. This system is capable of using several different alloys as feedstock, 17-4 PH is used in this thesis. Samples were printed by the company Aidro in Italy, using the shop system. The samples were sent to the University of Stavanger were heat treatment and subsequent mechanical testing and examination of microstructure was performed. The mechanical testing involved tensile testing, notched impact testing and hardness. Microstructure was examined using light optical microscope and scanning electron microscope.

2 Literature review

2.1 Additive manufacturing AM

The precise definition of the additive manufacturing has been vague. This is most likely a result of the fact that the technology is relatively new and there is a lot of research going on. Standards have been made available to clarify terminology. In ASTM/ISO 52900-21, additive manufacturing is defined as "Process of joining materials to make parts from 3D model data, usually layer upon layer, as opposed to subtractive manufacturing and formative manufacturing methodologies" [1, p. 1]. This implies the

involvement of Computer aided design CAD, this disqualifies processes like metal injection moulding MIM. In MIM, powder is fused together to form the part, but the geometry is defined by a physical mould. AM is considered synonymous with 3D printing [2, p. 755] [3]

Lipson & Kurman have compiled a helpful list of ten general principals concerning 3D printing [4]. They provide an overview of the current benefits and possibilities within 3D printing. They are the product of condensed viewpoints from interviews and research surrounding 3D printing,

1.Manufacturing complexity is free

There is no difference between printing a solid block and an intricate geometry. In conventional machining, added complexity often requires added operations and is therefore more time consuming which lead to higher costs.

2.Variety is free

In conventional machining, the design of a product is often constrained by the machine capabilities available for production. 3D printing allows for building of all shapes without ordering new machines or retooling.

3. No assembly required

3D printers can produce interlocked parts. This eliminates assembly of several pieces to form the final part.

4.Zero lead time

In 3d printing, a new part can be sent to printing with no change of setup.
Additionally, in conventional production, assembly of various parts is often necessary. Parts not made in house must be ordered and stockpiled. Lack of parts and shipping time increases lead time.

5. Unlimited design space

The 3D printer can make intricate geometries. There is no constraints from tool paths.

6. Zero skill manufacturing

The 3d printer eliminates the need for skill. Conventional machining requires a trained operator who understand the limits and abilities of the CNC machine. In 3D printing the user draws a CAD file, most of the technical printing parameters are handled by a computer.

7.Compact and portable manufacturing

A 3D printer is relatively small in regard to the amount of geometries it can generate. A conventional machine shop has large heavy equipment that often are limited to simple operations.

8.Less waste by product

In conventional machining excess material is removed from a solid billet to form a final part. The excess material ends up as shavings, often the weight of shavings are many times more than that of the product. In 3D printing particles are fused together to form final part, ideally there should be little waist.

9.Infinite shades of material

The 3D printing process allows for fine blending of different materials in the part.

10. Precise physical replication

The interface between the digital and physical world should be easier. 3D scanning and photography should allow for precise replication using a 3D printer. A part could be scanned, improved in a CAD program, and then printed.

There are off course negative sides to AM also. At the present time, the energy needed to create a part is high. The raw material is expensive. The time to build is time consuming. The mechanical properties are often lower that their wrought counterparts, due to pores or microstructure.

AM is subdivided into seven categories as described in ASTM/ISO 52900-21 [1, p. 2].

1. Binder jetting

2. Directed energy deposition
3. Material extrusion
4. Material jetting
5. Powder bed fusion
6. Sheet lamination
7. Vat photopolymerization

This thesis is concerned with the binder jetting method.

2.2 Binder jetting printing BJP

ISO/ASTM 52900-21 define binder jetting as ” additive manufacturing process in which a liquid bonding agent is selectively deposited to join powder materials” [1, p. 2].

The process from powder to finished part can be subdivided into separate processes

- Printing
- Curing
- De-powdering
- Binder pyrolysis
- Sintering

The printer has a surface area where the part is incrementally built on, this is called the build bed. A fine layer of powder is evenly spread across the build bed by a roller. The binding agent is applied onto the powder in the build bed, covering the part geometry. The binder is then allowed to cure slightly by passing an electrical heater across the build bed. The build bed is lowered an amount, before the next layer is applied and the process repeats until the part is done.

The next step is to cure the part, this is done to maximize the strength of the part due to the binding agent. In this state, the part is referred to as in the green state. This must be done to allow for de-powdering, where excess powder is removed by some mechanical action.

The next step happens in the furnace, this is a machine capable of high temperature and regulating the atmosphere. The binder must be driven out, this is done by the application of heat and partial vacuum.

After the binder has been driven out, the next stage is the sintering. The temperature is increased toward the melting point. The atmosphere is inert partial vacuum. The process were the particles fuse together and gradually grow together, reducing the initial voids into smaller pores, is called densification.

2.3 The allotropes of Iron

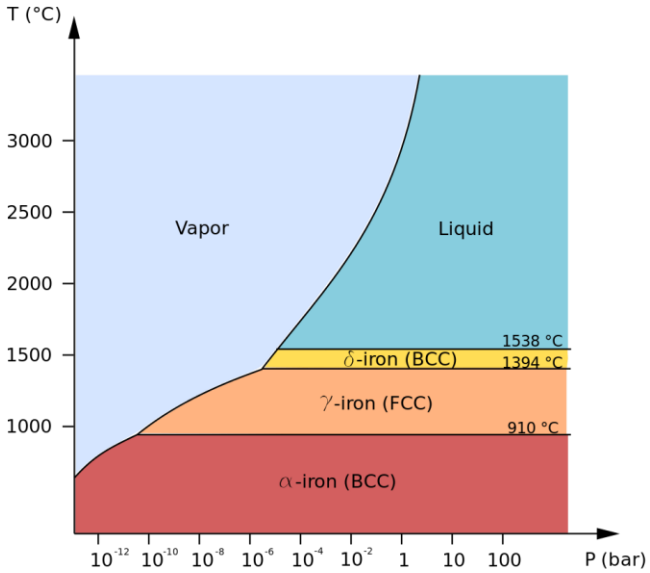

Figure 1 The allotropes of Iron is a function of temperature and presure [33]

In most stainless steels, the largest contribution of wt % in a given alloy is from Iron, Fe. Iron has several allotropes, which is the basis for all the different types of steel. In steelmaking there are two phases that are of primary interest, namely ferrite and austenite. The main difference between the two lie the way the atoms are crystallographically arranged. Ferrite has a body centered cubic structure (BCC) and austenite has a face centered cubic structure (FCC). Fundamentally, what allotrope iron will assume, is a function of temperature and pressure. It can be seen from figure 1 that there are two zones on the graph where iron has the BCC structure, they are crystallographically the same. The two zones are nevertheless differentiated, the upper zone is called the delta(δ) ferrite phase region and the lower region is the α(alpha) ferrite phase region. The gamma γ region with the FCC structure lie between the ferrite regions. There is at least one more allotrope, namely epsilon ε Iron. The crystallographic structure is hexagonal close packed (HCP), however iron does not appear in this form before extreme pressures.

One of the differences between FCC and BCC is the capacity to hold interstitial solid solution. The voids where interstitial atoms can manifest, are larger in the FCC structure. The size of a carbon atom is such that it can occupy interstitials positions.

The discovery of steel has had a large impact on human history in the last few centuries. The reason iron can be made into steel stems from the fact that it can be made to go through phase changes as a function of temperature. The γ phase can absorb more carbon into solution than that of the α phase, when cooled the carbon is not stable and starts to diffuse out of solution. This is the basis for the formation of cementite, together with the ferrite it makes the lamellar structure of perlite. If however the saturated γ iron was to be cooled very swiftly, then carbon would be trapped in the structure. This is the mechanism for the formation of martensite.

2.4 Martensite

Martensite is the result of a displacive transformation. Supersaturated austenite is rapidly cooled, the rate of cooling is such that the carbon is not able to diffuse and is trapped in place. The result is that the FCC phase transforms into the BCC phase, but because the carbon is still trapped in place the structure is strained slightly, into the Body centered tetragonal (BCT) unit cell. The amount of straining on the unit cell is a function of the amount of carbon in solution. It can be seen from figure 2 that, the BCT unit cell is distorted because of interstitial carbon.

Martensite is a metastable phase in the iron-carbon system. It forms by displacive transformation as a function of temperature. The reaction is not dependent on diffusion and can propagate rapidly, even under temperatures where diffusion is inconceivable.

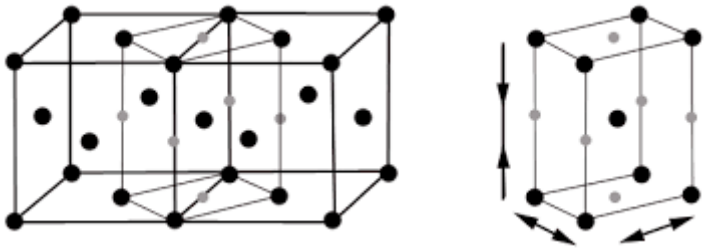

Figure 2 The displacive transformation of martensite [5].

Martensite appears in two main forms, highly distorted plate martensite and lesser distorted lath martensite. The structure always manifests within the boundaries of the prior austenite grain. If carbon is under 0.6 wt % then lath martensite will form. In lath martensite, the prior austenite grain is divided into several packets. Each packet contains laths of a certain crystallographic direction. The structure will be finer and less visible as carbon is decreased.

Higher amounts of carbon will promote so called plate martensite. Between 0.6 and 1 wt % carbon results in a mixed structure. Over 1 wt % results in a pure plate martensite. The amount of strain is so large that the martensite forms lenticular discs within the prior austenite grain. The explanation for this phenomenon is that the strain on the unit cell is very large. To minimize strain energy, the martensite develops a twin structure this manifests as a disc. Surrounding this shape is retained austenite.

Martensite is a hard and brittle microstructure. The brittleness can be remedied by tempering the martensite. This is done by heat treatment. The objective is to allow for carbon to precipitate out as cementite particles and a recrystallization of ferrite grains.

2.5 Stainless steels

The discovery and development of stainless steel happened in the early 1900s. Metallurgist where experimenting with using different elements in combination with iron. It was noticed that alloys containing chromium where resistant to chemical attack than regular carbon steel. [5, p. 3] The electric arc furnace was also invented in this timeframe, allowing for more alloying concentrations in the melt. It was found that the steel could be made to not rust in normal atmosphere conditions if the composition of chromium was over 11 wt%. The mechanism behind this inert property was discovered to be the reaction between chromium and oxygen on the metal surface, creating what is referred to as the passive layer. All stainless alloys rely on this chromium oxide layer to protect against corrosion. The passive layer can be compromised by formation of chromium-carbide, this depletes the matrix of chromium making it more susceptible to corrosion. This is called sensitization. Carbon must therefore be held to a minimum in stainless steels, or alternatively an addition of an element with greater affinity to create carbides can be added. Chromium content can also be elevated, in fact, the most common type of stainless steel has around 18 wt % chromium.

Stainless steels are separated into different categories. They are:

- Austenitic
- Ferritic
- Martensitic
- Duplex
- Precipitation hardenable

The first four categories differentiate the alloys based on the microstructure they have in room temperature. The last category indicates that the alloy can be hardened by precipitation of fine particles of solute from a supersaturated solution. The alloy is first solution treated to evenly spread the solute in the matrix, and then heated at a lower temperature to allow the particles to diffuse into particles. This is referred to as artificial aging. Alloys that are precipitation hardenable sometimes have this signified at the end of the designations with the letters 'PH' at the end. The PH category can overlap with any of the other four categories, there are three types of PH steels. Namely austenitic, semi-austenitic and martensitic. [5, p. 34]

The microstructures of the first four categories are the product of the alloying elements that make up their composition. Generally, alloying elements can be either γ (FCC) or α (BCC) stabilizers, the relative amounts of these will dictate the final microstructure. For instance, austenitic steels have alloying element composition that dictate that it will remain in the austenite phase regardless of temperature. Martensitic microstructure can be achieved if there is a phase transformation as a function of temperature. The duplex category is a microstructure consisting of ferrite and austenite , in relative equal amounts.

2.6 Effects of alloying elements

There are several aspects that one should consider when discussing the role of elements in an alloy

2.6.1 Interstitial and solid solution

Atoms with small radii relative to the matrix structure atoms, can go into interstitial solution. Nitrogen and carbon er the two typical elements. They are readily absorbed in austenite. Both elements are γ stabilizers. Atoms that have similar radii can form solid solutions with the iron atoms.

2.6.2 γ and α stabilizers

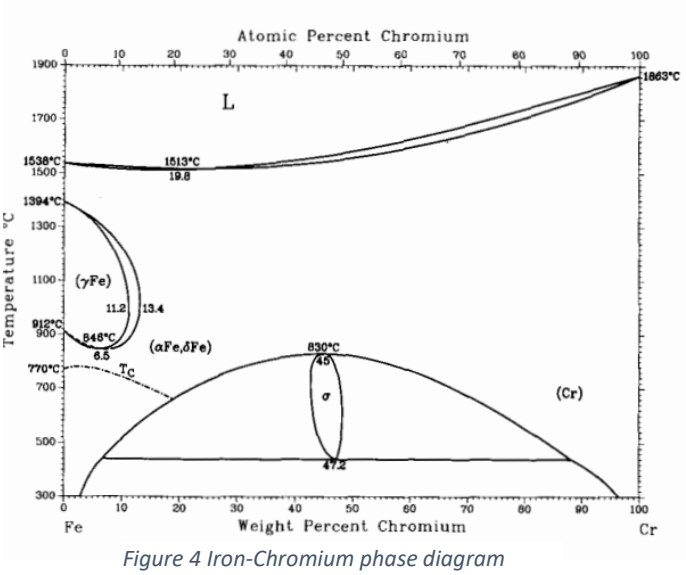

Figure 4 Iron-Chromium phase diagram

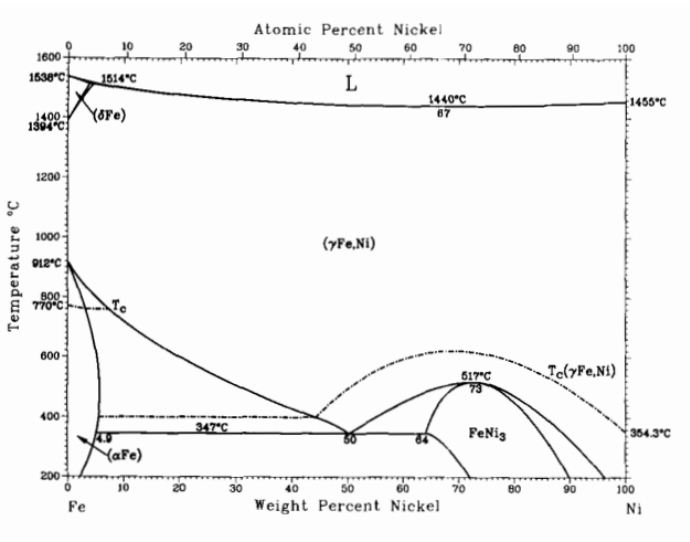

Figure 3 Iron-Nickel phase diagram asm vol 3 s.34

Iron is capable of changing phase as a function of temperature, however this can also be manipulated by solid solution elements. Chromium, for instance, is an element that readily forms solid solution with the iron matrix, chromium remains in BCC structure as the temperature increases. The effect it has on the matrix is said to be α stabilizing. It resists the matrix from changing phase to γ. The effect of chromium is evident when comparing figure.3 with figure 1. The γ phase region has been compressed into a small area when chromium is below 13.4 wt %. This phenomenon is called a closed gamma loop. When exciding 13.4 wt %, the δ and α ferrite region become one continuous region. [6, p. 104]

Table 1 Examples of phase stabilizing elements

α stabilizer	γ stabilizer
Chromium	Nickel
Molybdenum	Manganese
Titanium	Carbon
Niobium	Nitrogen

The opposite is seen with the addition of nickel as seen on figure.4 When nickel is added to iron, it will expand the γ phase region. It can be seen that the δ ferrite phase region is oppressed to a small region in the left hand corner. For the remaining composition, the γ phase region meets the solidus line. Nickel has FCC structure and therefore tends to promote this structure, it is said to be a γ stabilizer. Stainless steel alloys consist of more than two alloying elements, it is the combined effect that will dictate the resulting phase. Some elements are γ stabilizing and some are α stabilizing, and the potency is varying.

2.6.3 Austenite phase transformation

Some alloys will have an austenite phase region at higher temperatures and will undergo a phase transformation as the temperature sinks below the lower bounds of this region. The final microstructure is dependent on several factors. First to consider is the shape of the TTT- curve. Most alloying elements will tend slow down the rate of diffusion, moving the curve to the right relative to carbon steel. This allows for slower cooling rates, when forming martensite. [7, p. 190]

The shape of the curve is also subject to change, chromium and nickel in particular tend to suppress the upper pearlite region, allowing for the creation of Bainite. [7, p. 184]

The last factor to consider is the temperature range of martensite creation. Generally, elements in solid solution in austenite, tend to lower the transformation start temperature of martensite. The

interstitial elements, carbon, and nitrogen, have a greater effect. [6, p. 108]. Some alloys will have the transformation finish temperature below ambient temperature, this results in retained austenite.

2.6.4 Age hardening agents and carbide formers

Age hardening agents are elements that are intended to allow precipitation hardening of the alloy. Copper is one such element. Carbide formers are elements that have a strong affinity to form carbides. In stainless steel, this is particularly of concern, as carbon in the alloy will readily form carbides with chromium. This can lead to depletion in certain areas. Elements like Niobium, have a higher affinity than that of chromium, thus this helps avoid this problem.

2.7 The stainless-steel alloy of 17-4 PH

This thesis is mainly concerned with the stainless-steel alloy called '17-4 PH'. The designation reflects some of the alloying elements present. 17 wt % Chromium and 4 wt % Nickel. The PH signifies, as discussed earlier, that the alloy id precipitation hardenable. 17-4 ph lies in the martensitic of the steel categories. Precipitation hardeneable alloy are always classed based upon the microstructure in the solution treated state. The AISI designation 17-4 ph is the prevalent naming convention used in the AM-industry, other commonly used grade designations are: UNS 17400 , DIN 1.4542 and SAE 630.

Table 2 Composition of powderstock used as stated by Desktop metal [8]

Cr	Ni	Cu	Mn	Nb+Ta	c	Si	Fe
15.5-17.5	3-5	3-5	1.0 max	0.15-0.45	0.07 max	1.0 max	balance

The nominal composition is listed in the table above. Copper is the age-hardening agent. Niobium is added as a carbide former. The amount of carbon is low, the martensite structure is therefore a low strained lath type. The transformation start temperature is around 130 ^{o}C and the final temperature is around room temperature. The hardenability is good, quenching in air is adequate to produce the martensitic microstructure. The melting point is between 1400-1440 ^{o}C [5, p. 10]. Due to low amounts of carbon in the composition, the alloy is well suited for welding. Steel vendors will often state that the corrosion resistance of wrought 17-4 ph is comparable to that of type 304. [9] One important consideration that is relevant for most of the stainless steels is the so called 475 C embrittlement problem. 17-4 PH lay in the miscibility gap on in the iron-chrome phase diagram. Exposure to temperatures between 400- 550 ^{o}C over long periods of time, will lead to phase separation and embrittlement [10].

2.8 Microstructure of sintered 17-4 PH

There are numerous studies on the topic of the microstructure of sintered 17-4 ph. Much of this knowledge comes from metal injection moulding industry, which is similar in nature to BJP.

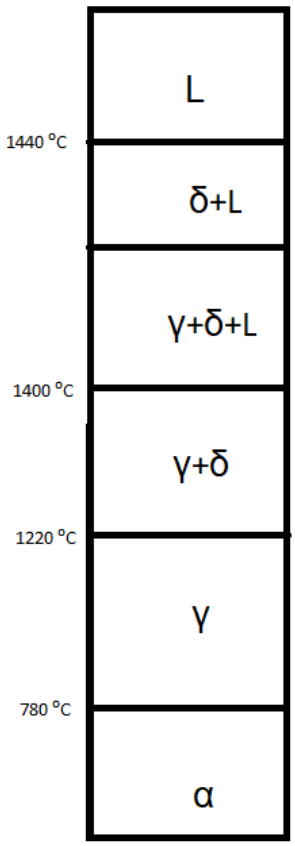

Figure 5 Approximate diagram showing phases.

The initial microstructure is a product of the manufacturing method. Generally, there is a dual phase mixture of ferrite and martensite. The sintering process starts by heating the green part up. As the temperature climbs towards 780 °C, there is a thermodynamical drive for the precipitation of γ-austenite. The volume fraction increases with temperature. At around 1200 °C the precipitation of δ-ferrite begins [11] [12]. The final sintering temperature is in the area just below 1400 °C [12] [13]. The δ-ferrite is thermodynamically more favourable than that of γ-austenite. δ-ferrite will thus gradually grow, nucleating from the γ grain boundaries. The process is sluggish because the mechanism behind the phase transformation is solid solution diffusion of γ- and δ stabilizers across grain boundaries. Consequently, this is the explanation why δ-ferrite is so prevalent in sintered 17-4 ph. To reverse the process, removing δ-ferrite would require soaking time in the temperature range where γ-austenite is favourable. This is a considerably lower temperature, so solid solution diffusion is slower.

Copper is one γ-stabilizer that diffuses over to the γ-phase during this process, leaving the δ-ferrite with a lower composition of copper. Nickel also has the FCC lattice structure and tends towards the γ-phase. Chromium on the other hand has BCC lattice structure, so it diffuses the other way enriching the δ-phase. When sintering is complete, the temperature will start to decrease. δ-ferrite will partially convert to γ-austenite, the speed that this happens slows down as diffusion is temperature dependent. Bellow around 780 °C, γ-austenite becomes thermodynamically unstable [12]. If the rate of cooling is within critical cooling rate, γ-austenite will start to transform to α' -martensite at around 130°C . M_f is typically stated to be around room temperature. The final structure consists of lath martensite inside the prior γ-austenite grains. Surrounding these grains is the remaining fraction of retained δ-ferrite. One crucial point to underline is the fact that solubility of copper is lower in BCC/BCT so the martensite now is supersaturated with copper. [11]

It is well established that a crucial factor behind the densification process, is the amount of δ-ferrite in the microstructure. Pores that are in contact with δ-ferrite tend to shrink at a higher pace, this is attributed to the fact that there is an increase in mass-transport pathways and a higher diffusion rate in ferrite generally [12]. Because of this the alloy and sintering process must therefore be tailored to allow for a high enough fraction of δ-ferrite. One factor that can offset the desired development of δ-ferrite, is absorption of γ-stabilizers during the manufacturing processes. Examples are during the gas atomization of the powder feedstock, from the gas used in the furnace atmosphere or residual binging agent. Nitrogen and carbon are the main elements of concern. Absorption of these elements will expand the γ-phase field, thus the temperature region where δ-phase precipitates is minimized and will start at a higher temperature. Wu et al [12] demonstrated this by comparing sintering atmospheres over different temperatures. It was found that the atmosphere containing nitrogen

slowed the densification process down. Wu et al [13] also found that residual carbon had e detrimental effect on densification, de-binding at higher temperatures tended reduce the amount of residual carbon, improving densification.

2.9 Heat treatment of 17-4 PH

The mechanical properties of 17-4 PH can be manipulated by heat treatment. It is a twostep process. The first step is called the solution treatment. The material is heated up to around 1050 °C and allowed to soak for a given time. The goal is to convert the α' martensite to γ-austenite, and for the solid solution elements to disperse evenly in the matrix. The soaking time is dependent on the thickness of the material. When soaking is complete, the material is quenched, resulting in a supersaturated martensitic structure. The displacive transformation causes dislocation buildup in the δ-ferrite grains, resulting in a brittle structure [11]. The part is now solution treated, it is said to be in condition A.

The second step is called aging. Aging is the process of letting reactions manifest in the microstructure as time goes on. If the aging happens at room temperature, it is called natural aging. 17-4 PH calls for elevated temperatures, this is called artificial aging. The reaction that is occurring is twofold, first the martensite is tempered and secondly, the precipitation of fine copper particles. The temperature range that aging can be done is from 482°C to 760°C for soaking times typically one or four hours. The industry standards that are in widespread use the naming convention based on the aging temperature in Fahrenheit. For example H900 signifies that it aged at 900°F, which is 482°C. The ASTM standard A693-16 [14] defines the solution treatment and aging regimes for 17-4 PH and other alloys.

Two aging regimes are used in this thesis. H900 is the aging regime that should result in maximum hardness. The soaking time is defined to be one hour, and the temperature is 482 °C. Copper has started to precipitate, they form small clusters and are still coherent with the surrounding matrix. The strain that this puts on the lattice hinders the movement of dislocations. The copper particles grow as a function of time and temperature. The second aging regime is H1150, the aging parameters are 621°C, for four hours. Both tempering of martensite and clustering of copper is increased. The copper particles have grown to such a size, that they take on a FCC structure and the coherency with the matrix is lost. In fact it is found that these copper clusters tend to manifest at the lath boundaries of the martensite, which in turn has lead to the reversion to austenite. Resulting in a lamellar structure of austenite and tempered martensite [11] [15] [16]. The result is an increase of ductility at the expense of hardness.

2.10 Mechanical properties

2.10.1 Modulus of elasticity E-module

In the tensile strain-stress curve, the linear portion before the material starts to plastically deform, is called the elastic region. If a material is loaded within the bounds of this area, the material will spring back to original form. The slope of this straight line is called the modulus of elasticity. A steep slope implies a stiff material, in the sense that more stress is required to strain. [17, p. 214]

2.10.2 Strength

Strength is a measure of a given materials ability to withstand stress. The point at which the material starts to plastically deform is called the yield strength.

The maximum point in the engineering stress-strain curve is called tensile strength. [17, p. 220] The unit of measure is often in Megapascal MPa.

2.10.3 Ductility

A material that undergoes plastic deformation when loaded axially, the material is said to be ductile. The opposite of ductility is brittleness. A brittle material will show very little plastic deformation, as a consequence of this behavior, fracture can occur in close proximity to the yield point. Ductility can be reported in several ways, however, this thesis will only elaborate on ductility through percent elongation, which is the lengthwise increase, in percent, from the original gauge length. A material is considered to be brittle if the elongation to fracture is less than 5 % [17, p. 224]

2.10.4 Toughness

Toughness can be an ambiguous term. In this thesis, toughness is limited to mean the property that describes a materials ability to endure both strain and stress. A brittle material is said to have low toughness, because while it may display high strength, it fails after minimal straining. Toughness can be gauged using different methods, and they will produce different values. Temperature, Strain rate, Notch effect are the main factors that have a large impact on the results [17, p. 300]. Toughness can be visualized by studying the tensile stress-strain curve, the area under the curve quantifies the inherent toughness in the material. Calculating this area will result with a unit of Megapascal, this unit can be rewritten to energy per unit volume, which is how toughness typically is reported. Another way to quantify toughness is through impact testing. A hammer strikes the specimen with a notch, causing a high strain rate, and resulting in fracture. The energy that the fracture absorbs is indirectly attained from the observed loss of energy in the pendulum. Some materials can undergo a transition from high to low toughness as a function of temperature, however this is beyond the scope of this thesis.

2.11 Tensile test

Tensile testing is a test where a sample is axially stretched until it breaks, some of the properties which can be attained from this procedure are Yield strength, ultimate tensile strength UTS, E-modulus, reduction of cross section % and elongation. Continuous stress and strain data can be plotted to produce a curve. This is known as the engineering strain-stress curve, because the cross section is not continuously updated.

A sample which is not brittle in nature will tend to progressively become thinner as the test converges towards the breaking point. This is called necking, and it is not accounted for in the data. We thus refer to this as engineering stress and strain, the data reflects true stress and strain on the first part of the data when the surface area is unaltered.

2.12 Charpy v-notch CVN

Impact toughness is a materials ability to elastically deform when subjected to stress at a high rate of straining. A material low in toughness is said to be brittle, it fractures with little deformation. A common way of determining this property is by notch impact testing, where a standardized piece of material is placed in a machine where a hammer swings down like a pendulum. The piece is broken, and the thougness of the material determines how much energy is absorbed from the kinetic energy of the hammer. A notch is carved into the test piece so that the fracture propagates from the same place in all testing. The amount of energy lost by the cleaving action can be recorded an indicator .

2.13 Hardness testing

Hardness of a material is the measure of the resistance against deformation when a concentrated stress is applied to the surface. Vickers hardness test is one method used. It works by applying a pyramid shaped diamond on to the surface of the material for a given period of time and with a given load. A softer metal will result in a deeper indentation, this is measured by measuring the length of the two diagonals produced. Vickers hardness can be calculated using:

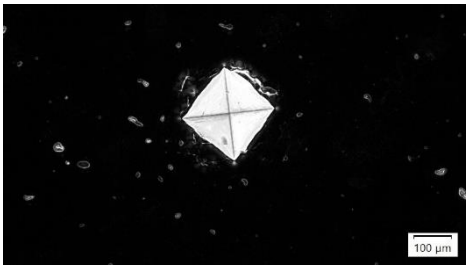

Figure 6 LOM showing diagonals of indentation. Taken using Darkfield mode

$$HV = 1.854\frac{P}{d^2}$$

From the formula, P is the loading in Kg and d is the mean diameter of the two diagonals from the indentation. The resulting unit for Vickers hardness is kg/mm^2.

2.14 Light optical microscopy LOM

The light optical microscope can be used to study the surface of metals. An image collected by use of LOM is referred to as a micrograph. The surface must be polished such that light can be reflected of the surface. Contrast in the image is a result of the fact that different microstructures reflect light slightly differently. The reflected light from the sample passes through the objective lens to form the primary image. Another combination of lenses called the ocular or eyepiece then magnifies the primary image producing magnified view. [18, p. 103]

There are two ways of directing the light when viewing the specimen. In bright-field illumination, the light is directed normal to the surface. Dark areas are areas reflect light at an angle so it misses the objective lens. Dark-field illumination is when light is directed not normal to the surface, a surface that reflects light at an angle is more probable to hit the objective lens. Dark-field is therefore optimal for studying surface with texture.

Further contrast in the surface microstructure can be achieved by applying an etchant to the surface. Etchants work by reacting with the surface textures at different rates. Grain boundaries tend to be highly reactive in comparison to the grains. Different grain orientations are also effected slightly differently, a crystallographic orientation that is misoriented to the surface is more susceptible to chemical attack than a surface that is crystallographically parallel.

2.15 Scanning electron microscope SEM

The main principle behind SEM, is that electrons are fired at the surface of a specimen. These electrons will interact with the atoms on the surface, and information can be gathered by recording the various signals that the excited atoms emit. The electrons fired are called primary electrons and are fired from the electron gun. The electrons are accelerated through a condenser to give them high energy. The primary electron beam is run across the interest area in a raster scan method. The samples must be clean and must be able to withstand the vacuum atmosphere, another important

note is that the specimen must be electrically conductive and grounded to dissipate the charge build up.

2.15.1 Secondary electrons SE

Secondary electrons are electrons that are knocked of the specimen atoms, they are relatively low in energy. Because of their low energy, they have little penetrating capacity under the surface. The electron detector will therefore only detect secondary electrons that emanate in close proximity to the initial electron beam, resulting in a high-resolution image. This gives the capability of mapping the topology of uneven surfaces, for example fracture surfaces.

2.15.2 Backscatter electron BSE

Backscatter electrons are electrons that are scattered elastically, meaning that they are the primary electrons, but their trajectories have been altered after interacting with atoms in the sample. These electrons have higher energy than that of SE, thus they can propagate deeper trough the material. This means that the resolution will be poorer when picking up BSE. The signal of BSE on a given point is related to the atomic number of the atom, higher Z numbers give a higher probability of BSE. Heavier elements will appear brighter compared to surrounding lighter atoms. Lighter elements will appear darker. BSE can display local variations in atomic numbers.

2.15.3 Energy dispersive spectroscopy EDS

The primary electrons can interact with a surface atom in such a way that, an electron is knocked of, typically from the k shell or L shell. The atom is unstable in this state, and a electron from a higher shell will fall down to replace the vacancy. This results in a discharge of an x-ray photons, the energy of the photons are characteristic to the atoms they emanate from. EDS gives the capability of qualitative composition analysis of pinpointed areas on the specimen surface.

2.16 Fractography

Information about a materials properties can be ascertained by analyzing its fractured surface. Observations can be gathered in a wide range of ways, from visually observing directly with eyesight, to electron microscopy. This thesis is mainly focused on fractography by way of SEM.

SEM allows for studying the fine topology of the fracture surface. Generally, the observable features on the surface can be regraded as evidence of ductile or brittle fracture. However, this can be misleading as these features often appear in combination.

2.16.1 Dimples

The presence of dimples is an indicator of ductile fracture. When a material is subjected to a tensile load the material starts to stretch. Small microvoids start to nucleate from imperfections, like an inclusion. The voids grow in size, and when they coalesce they have effectively separated the material allowing the crack to propagate. The resulting surface left behind has the characteristic half spheres, this is referred to as dimples. The mechanism of micro voids coalescing to become a crack is referred to as microvoid coalescence, MVC. The dimples will sometimes contain an inclusion, this is the point of nucleation. [19, p. 66].

2.16.2 Intergranular fracture

Fracture displaying granular features, the fracture has followed the grain boundaries is referred to as an intergranular fracture. Its presence indicate a brittle fracture. [19, p. 70]

Possible reasons for intergranular fracture is the weakening of the grain boundaries. This can happen through for example ,hydrogen embrittlement or stress corrosion cracking, these mechanisms attack the high energy grain boundaries. The topology of this kind of fracture resembles that of rock candy.

2.16.3 Transgranular fracture

The fracture occurs along the crystallographic planes instead of following around the grain. The fracture mode is therefore often referred to as a cleavage fracture. The direction of crack propagation will often not coincide with the crystallographic plane inside the grain, so the crack must shift between parallel layers to maintain the direction of the crack travel. This is the explanation behind the river phenomena that is typically associated with cleavage fracture. The direction of crack propagation can also be ascertained by studying the rivers. Flowing from the branched end to the thicker end. [19, p. 64] Another feature that can be found on a cleavage face is a so called tongue. Tongues appear as thin layers on the cleavage face, they are the result from when the cleavage start to follow a twingrain orientation for s short while before falling back to the original plane.

A material that does not have clear cleavage plane, like that of a martensitic structure, is said to display quasi cleavage fracture faces. The surface can consist of smaller fragments of quasi cleavage faces, initiated by surface defects in the material.

3 Experimentation

Some effort was spent trying to find relevant testing standards to follow for mechanical testing. Inspiration was found in a previous thesis [20] were a standard from Det Norske veritas DNV was used. Namely DNVGL-ST-B203 [21]. It contained some recommendations regarding what specific test standards to use.

3.1 Shop system by desktop metals

The samples were made at Aidros facility in Italy using the Shop system by Desktop metals.

The shop system consists of four modules

- Printer
- Drying oven
- Powder station
- Furnace

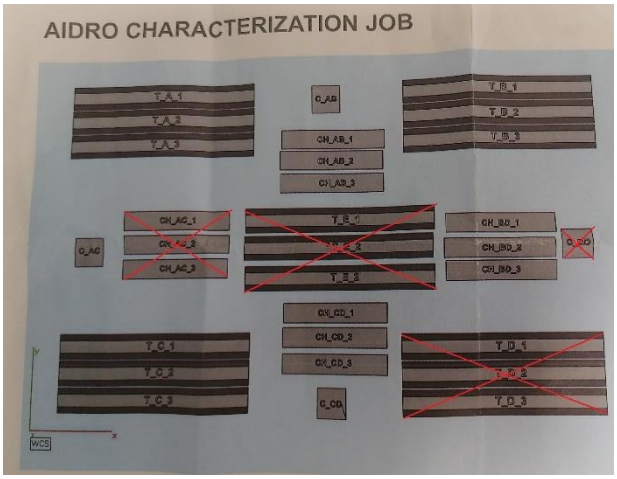

Figure 7 Work draft displaying the printing job. The crossed out samples are not involved in this thesis

3.2 As- received samples for Aidro

The samples were then shipped to Norway.

There were three different types of samples made. The tensile tests had a hexagonal cross section a length of 100 mm and a face diameter of 11 mm. The Charpy samples were printed to dimensions 10mm x 10 mm x 55mm. The cube had 15 mm sides, and its purpose is for taking micrographs and hardness tests.

Figure 7 show a plan of the build bed, crossed out samples were not used in this thesis.

A system was created, its purpose was to protect the samples and preserve the identities of the samples. The samples could easily get mixed up during some operation.

The system was two sets of fising lure boxes. The samples were also individually put into a marked ziplock bag, this would avoid mix up should the boxes be accidentally dropped on the floor.

The samples were assigned a heat treatment according to Table 3.

The term As printed, means that no further treatment was done to it after leaving the sintering oven at Aidros facilities.

Figure 8 Fishing lure box. Containing the tensile specimen.

Table 3 Heat treatments assigned to specimen

Heat treatment	Specimen type	Aidro name
As printed	Tensile	T_A_1 T_B_1 T_C_1
	Charpy	CH_AB_1 CH_BD_1 CH_CD_1
	Cube	C_AB
H900	Tensile	T_A_2 T_B_2 T_C_2
	Charpy	CH_AB_2 CH_BD_2 CH_CD_2
	Cube	C_CD
H1150	Tensile	T_A_3 T_B_3 T_C_3
	Charpy	CH_AB_3 CH_BD_3 CH_CD_3
	Cube	C_AC

3.3 Heat treatment

The heat treatment was performed in the heat treatment department at Kverneland groups plough factory in Klepp, Norway. The oven was industrial furnace made by C.H Evensen A.S The atmosphere was made inert by argon purging and the temperature was monitored using a thermocouple.

The aging process was performed in a different oven. This oven did not have the inert gas feature. In order to avoid scaling. The part was wrapped in stainless steel foil, aisi 321, with some tissue paper. As the temperature increased, the paper combusted and thus oxygen was consumed. The aged parts have a sotty appearance because of this.

Figure 9 Removing the samples from the oven after solution treatment.

3.4 Charpy v notch CVN

Machining was performed by a machinist at the university mechanical workshop. The parts requiring machining where the tensile tests and the charpy notches. Work plans where drafted in Inventor.

The machine used was the Genos L3000-e made by Okuma. The machine uses coolant avoiding overheating. The tensile tests where individually turned down to size and threads where made in the ends. The Charpy specimen where all printed to size, so nothing more was done to them other than machining in the notch. The charpy specimen where all cut at once, they were placed in a jigg and a cutting wheel was run across them.

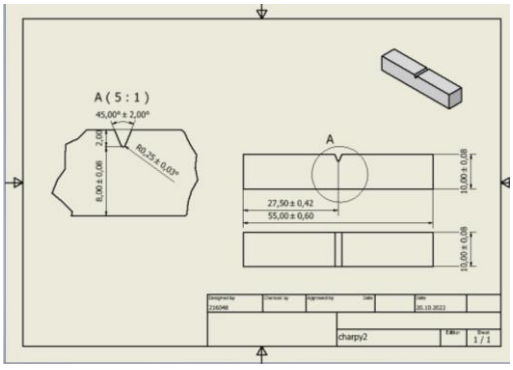

Figure 10 CVN workdraft for machining

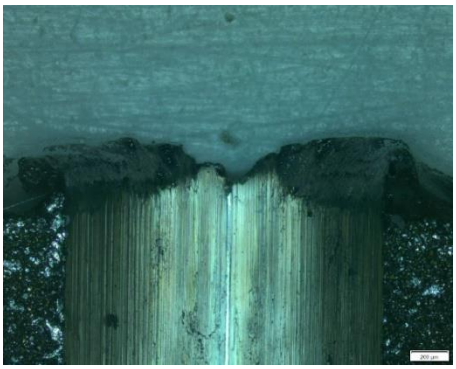

Figure 11 Bur after machining

When inspecting the specimen after machining, it was found that the cutting operation had left significant burs on the charpy specimen as shown in Figure 11. The bur was removed by placing the specimen in a jigg that allowed for filing the burr down.

The finished specimen were analysed using the LOM. The radius of the notch was inspected, and no defects were found on the surface.

DNVGL-ST-B203 suggested the use of ISO148-1:2016 [22]. Additionally notch parallel to the build direction.

The final dimensions of the specimen were measured using callipers. The final dimensions can be viewed in the appendix

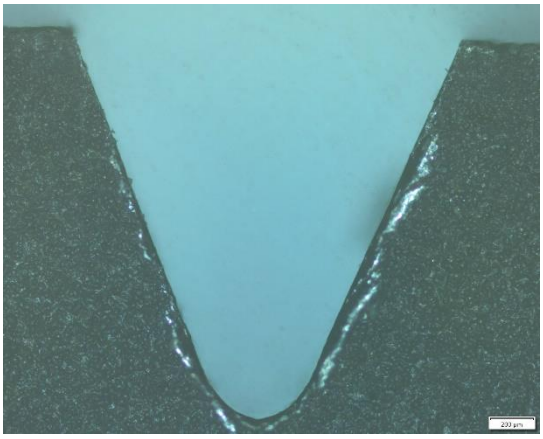

Figure 12 LOM image showing V-notch

3.5 Tensile testing

The machine being used is an Instron. The interface software is Bluehill 3.

The standard selected for carrying out the tensile testing was ASTM E8M, which was one of the alternatives suggested by DNVGL-ST-B203.

Because of the dimensions of the as-received specimen. It was decided that the final dimensions after machining should conform to “Specimen 3” Under the “small-size specimens proportional to standard” [23]. This would result in a test piece with a diameter of 6 mm, and a gauge length of 30mm which is five times that of the diameter. The reduced parallel length was chosen to be larger than 36mm, the standard allows for a longer reduced parallel length to accommodate an extensometer. A length 56 mm was chosen, the clip-on extensometer had a gauge length of 50mm.

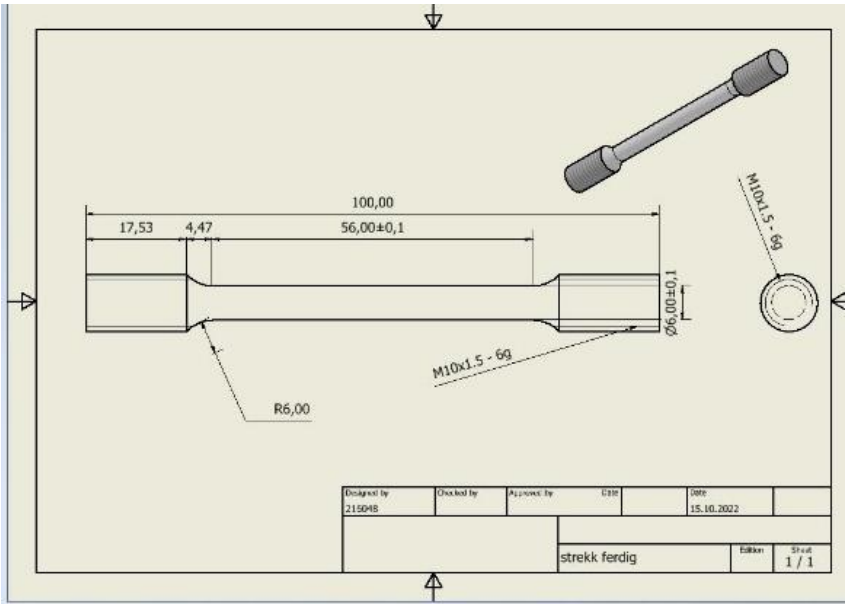

Figure 13 Work draft tensile

The specimen ends were machined with M10 external threads. Solid steel cylinders where found in the lab from a previous experiment, the cylinders had internal M10 threads. These cylinders had a larger diameter and sufficient length so that the friction grips on the tensile machine would get an optimal grip thus avoiding slippage. The tensile test would simply have a steel cylinder screwed in on both ends, the cylinders would interface would the machine grips.

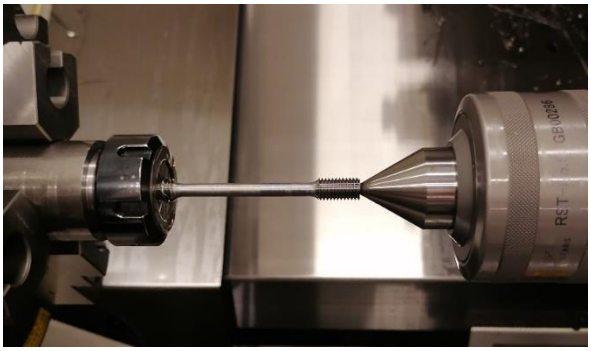

Figure 14 Machining tensile specimen

The machine used for CNC machining was the Genos L3000-e made by Okuma. The machine uses coolant during operation avoiding overheating. The tensile tests where individually turned down to size and threads where made in the ends

The tensile test consists of two main parts. The first stage is determining the yield properties and elastic modulus of the material. Initial testing had indicated that yielding occurred in a continuous fashion. The relevant settings was selected in Bluehill 3, the software would detect when the yield point was reached and the machine would proceed to the next stage which is determining the tensile strength and elongation until fracture.

The first stage of the test calls for a slower strain rate than that of the second stage. The rate at which strain occurs can vastly influence the resulting strain-stress profile, so making sure the machine is working consistently within the allowed tolerance is key to obtaining good results.

Stage 1 was conducted under 7.6.4.2 “Control method B- Rate of straining control method for determining yield properties” The allowed strain rate is 0.015 +/- 0.006 mm/mm/min. A removable clip-on extensometer was used at this stage. Once yield point was detected, the software would display a notice, allowing the operators to remove the extensometer before the test would transition into stage 2.

Stage 2 was conducted according to 7.6.5 “speed of testing when determining tensile strength”. The allowance for strain rate is between 0.05 and 0.5 mm/mm/min. Going from phase 1 to phase 2, the strain rate ha to transition, the software calls this a ramp up.

Initial testing had indicated that the strain rate could sometimes overshoot the allowed tolerance, this would typically happen during ramp ups. The machine would sometimes overshoot and overcorrect, thus yielding a noisy strain rate profile. Trial and error resulted in selecting the parameters that seemed to minimize these effects.

Stage 1 had a target strain rate of 0.015 mm/mm/min and stage 2 was set at 0.1 mm/mm/min.

One feature on the Instron machine is called “specimen protect”, this ensures that unwanted pressure is minimized. For instance, tightening the machine grips that hold the specimen could impose some unwanted pressure. Specimen protect self-adjusts dynamically when such forces occur.

Before the testing could begin. The clip-on extensometer was calibrated and the load cell was balanced.

Every specimen was inspected before fitting into the machine. The diameter and length was meticulously measured using calipers, the surface was inspected for defects.

Figure 15 Tensile test post fracture

After each test, the fracture surface was photographed. The pieces where carefully released from the threaded cylinders, and put into a make shift jigg. This ensured that the identity of the two pieces was maintained and that the fracture surfaces where preserved for future fractography analysis.

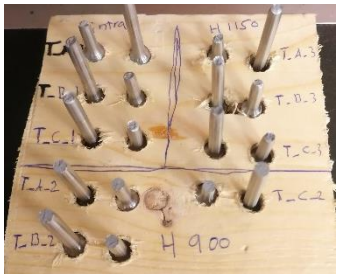

Figure 16 Broken tensile samples

3.6 Polishing sequence

Table 4 Regime of polishing discs and agents in polishing sequence

Disc name	Grit/polishing agent	Time
Piano	220	2m
Allegro	All/Lar	3m
Dac	Dac	3m
Chem	OP-AA	2m

The specimen were hot mounted in Struers Clarofast resin, this made it easier to observe the orientation since it is completely transparent. The mounting machine was a Struers Citopress-30. The specimen surfaces were polished using a Tegra system, made by Struers.

The program used to polish the specimen was an integrated method, called Method D. The last step in this method OP-S, this was changed to OP-AA because of availability. Due to the fact that 17-4ph is ferromagnetic and the base plate of the TegraPol is magnetic, a lot of care had to be made to clean the magnetic surfaces. The 17-4 PH dust will not wash away without mechanically wiping it off.

Failure to do this would ensure contamination of coarse particles onto the finer polishing plates, thus resulting in scratched surfaces. The samples were washed in between the polishing steps, and cycled through Struers Lavamin. Which uses ultrasonic cleaning and centrifuge.

3.7 Etching procedure

Table 5 Chemicals in Fry's etchant

HCL	40mL
CuCl2	5g
Water	30mL
Ethanol	25mL

Etching of the fine polished surface can help to reveal different phases and grain orientations. The mechanism behind this is that the etching agent reacts with the surface at different slightly rates. By studying previous studies and on recommendation from other students, it was decided to try the etchant called "Fry's etchant" . It is listed as etchant nr. 79 in ASTM 'Standard Practice for Microetching Metals and Alloys' [24, p. 20]. The components where mixed and stored in airtight brown glass container.

The surface was washed with alcohol and dried in an air dryer. The etchant was applied using a pipette. Time was recorded using a stopwatch. To stop the etching, the samples were washed under running water, then rinsed with alcohol and dried. The degree of etching on the three sample surface varied, it seemed that the AP required the longest amount of working time. H1150 needed significantly less. It was also noted that etching time was generally shorter when etching was performed immediately after polishing.

3.8 Light optical microscope LOM

The apparatus used was the GX53 by Olympus. The live picture was displayed on a big screen, making it easy to use. The samples were mounted and polished to mirror finish as described above. Etching was done to reveal the phases. Micrographs were captured and marked using the Software Olympus Stream. The LOM was also used to inspect specimens and hardness indentations.

3.9 Scanning electron microscope SEM

The SEM machine was a Supra 35VP made by Zeiss.

It was decided that the samples for SEM should be compatible with the XRD machine. That meant a size limitation of 5 mm in height. The yz face of the cube was used, a slice was cut of using the Accutom cutting machine. The samples where then hot mounted in clarofast and cycled through the polishing sequence. The next step was to retrieve the metal samples without damaging the polished surface. This was attempted by packing it in cloth and crushing the clarofast using a bench wise, being careful not to crush the metal.

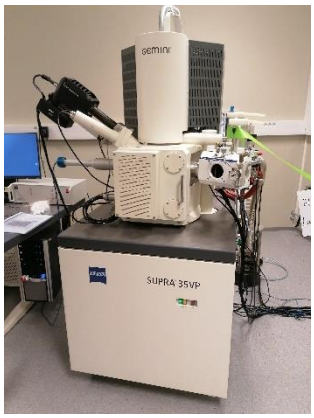

SEM

The samples were taped to the sample holder using conductive carbon tape, so that charge would dissipate. The first in attempt in the SEM worked fine for the AP sample, but the H900 and H1150 samples showed evidence of charge buildup. It was concluded that the light scale layer from the ageing process was to blame, not allowing for charge to flow to the carbon tape.

The samples were roughly grinded around the corners using Knuth-Rotor 2 made by Struers. The disc was a wet 600 grit disc. The samples were put through the polishing cycle once more, extra care was taken when removing from the Clarofast.

The second attempt resulted in clear images without charging lines. The surface was inspected using BSE, this allowed for locating and further EDS analysis of particles. EDS analysis was also conducted on the general matrix of the grains.

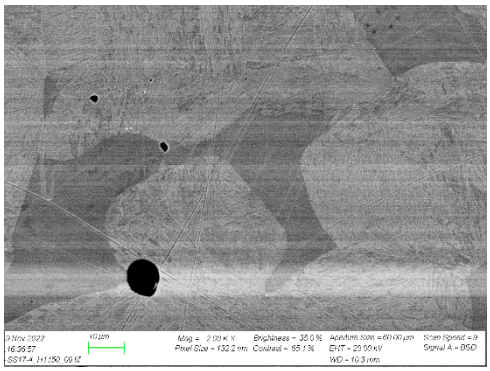

Figure 17 Poor grounding of sample, leads to poor SEM imaging

3.10 Hardness testing

The standard used for hardness testing was ISO 6507-1 Metallic materials Vickers hardness test [25]. This was one of the standards suggested by DNVGL-ST-B203, additionally the load was specified as HV10.

The testing machine used was Nova 330 made by Innovatest. The specific machine that was used to carry out the test was modified such that a small camera relayed the microscope image onto a computer screen making it more comfortable for the operators.

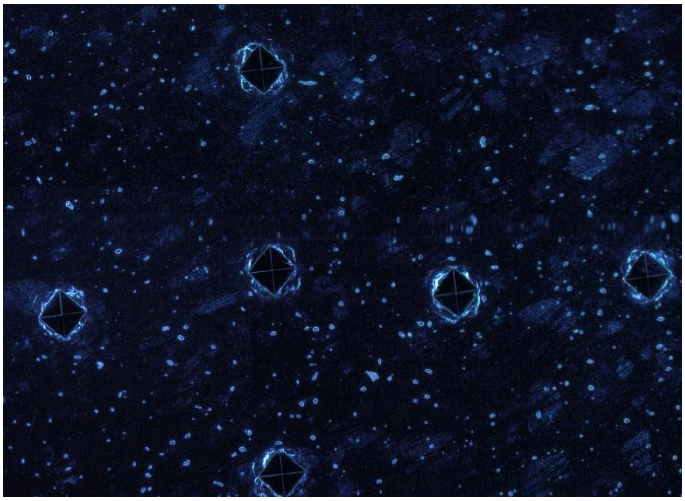

Figure 18 Hardness testing performed. Taken with LOM in darkfield mode

It was decided that hardness tests should be conducted in all three axis and that they should not be close to the original surfaces.

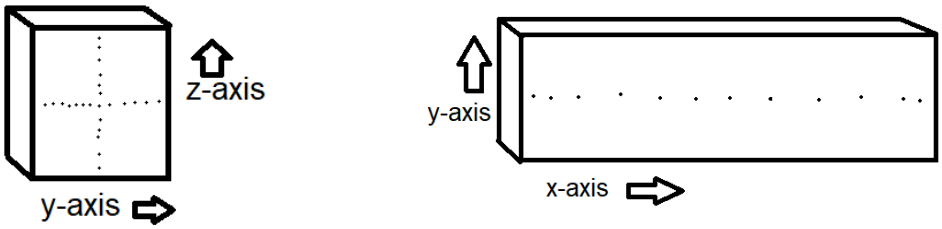

Showing the orientation of indentations on surfaces

The cubes were cut into halves using Discotom-10 made by Struers. This exposed a face that held the YZ axis. A suitable face that had the X axis in it was taken from the broken charpy pieces. It was divided into halves length wise using Accutom-5 made by Struers. The face was XY axis.

The measurements along the y and z axis were conducted on the same sample face, perpendicular to each other. The measurements were done at least 1,5 mm from the edge of the sample, and with a spacing of 1 mm between individual indentations.

The samples were put in a steel cylinder for stability.

3.11 Fractography

The broken pieces from impact and tensile testing where carefully stored, so as not to disturb the fracture surfaces. The pieces had to be sawn down in length to fit into the SEM. Using a fine-tooth hacksaw, the fractured end was separated from the pieces, approximately 1 cm in length. The sawing was done slowly and by hand, to avoid heat building up in the sample. For transportation and safekeeping, the samples were wrapped in tissue paper and put in marked compartments in a fishinglure box.

One of each heat treatment was fixed to the sample holder using carbon tape. A total of three tensile and three CVN specimen were loaded in the machine. The surfaces were studied capturing secondary electrons.

Figure 19 Carefully removing fracture end from the broken tensile specimen

4 Results

4.1 Hardness testing

A total of 117 indentations were done and measured, 13 for every axis of a given heat treatment. The averaged data and standard deviation for every given axis, each with the three conditions is represented in the bar chart below.

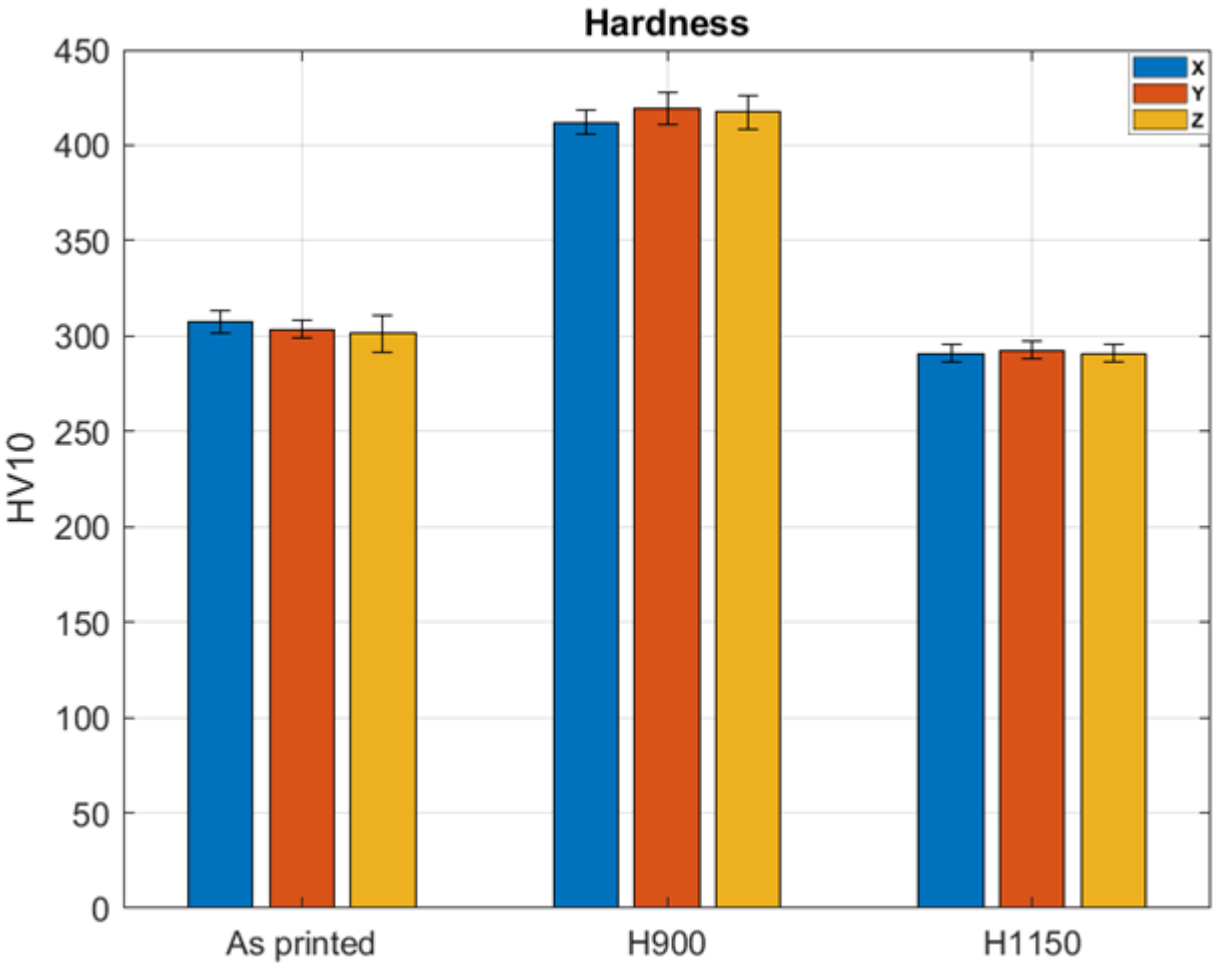

Figure 20 HV10 values for each direction in all of sample conditions

The hardness measurements seem to imply that the material is isotropic, the highest standard deviation was found in the As-printed samples in the z-direction. Standard deviation in the z-axis seemed to dissipate as with increasing aging. However an increase is observed in the H900 y-axis when comparing the as printed and H900 conditions.

The compounded average and standard deviation for each condition is presented in the table below.

Table 6 All directions compounded for each specimen condition

Condition	As printed	H900	H1150
Avg [HV10]	304.0	416.2	291.5
SD [HV10]	7.11	7.90	4.60

4.2 Tensile testing

As expected the highest strength values are obtained by the H900 condition specimen.The largest elongation was seen in the H1150 specimen as seen in Table 7.This condition also showed signs of strain hardening as seen on Figure 21. Toughness, which is visualized as the area under these curves on the stress strain graph was highest in the H1150 condition.

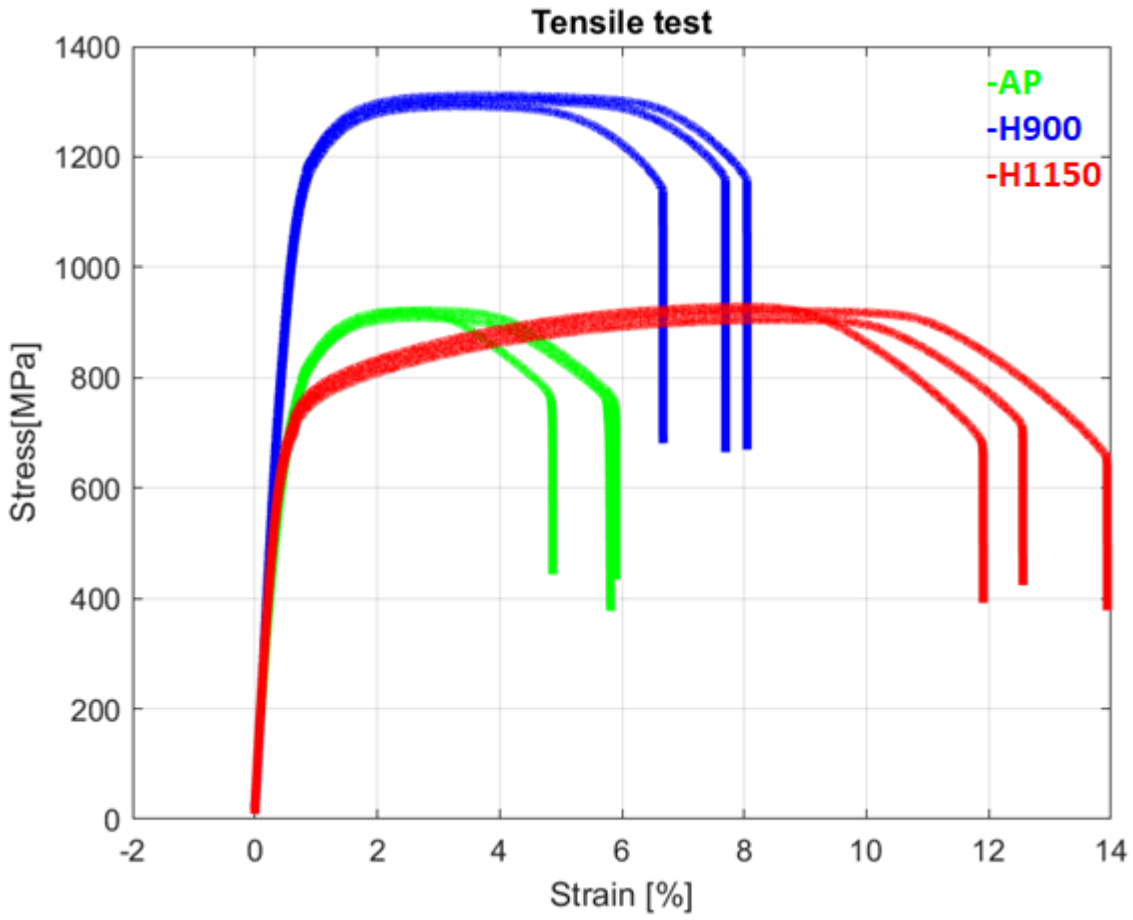

Figure 21 Engineering Stress-strain curves for tensile specimen

Table 7 Tensile properties for each specimen condition

Condition	Yield 0.2% offset [MPa]	E-Modulus [GPa]	Tensile stress [MPa]	Elongation [%] /50mm
As printed	788.1 +/-5.02	123.1 +/- 1.91	916.8 +/-6.65	5.5 +/- 0.57
H900	1162.2 +/-8.51	173.5 +/- 2.36	1301.5 +/- 8.93	7.5 +/- 0.91
H1150	706.9+/-12.36	150.3 +/- 1.67	917.5 +/- 11.33	12.8 +/-1.04

4.3 Charpy V-notch CVN

The h900 samples displayed the lowest impact toughness values. It was observed that the two pieces flew in a backwards direction in comparison to the travel of the hammer. This was though to be attributed the brittle nature of the fracture. In the other heat treatments, AP and H1150, the broken pieces flew forward together with the hammer.

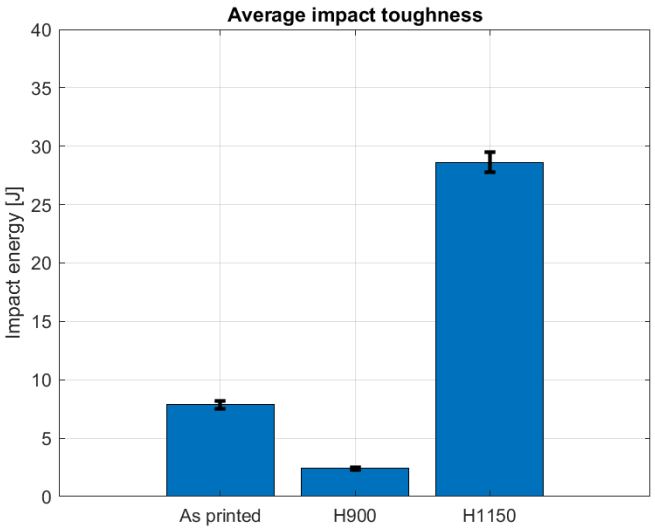

Figure 22 Values from Table 8 visulized

Table 8 Average CVN values for each specimen condition

Condition	As printed	H900	H1150
Avg [J]	7.9	2.4	28.6
SD [J]	0.40	0.17	1.01

4.4 Microstructure

The micrographs revealed that the microstructure consist of two phases. The literature has implied that the presence of δ-ferrite and α'-martensite is to be expected. Figure 8 shows EDS analysis of the two matrixes reveal that there is a difference in composition of Chromium and γ stabilizing elements between the phases. This information is useful as to ascertaining the identity of the phases. The specimen used in the analysis is the H900 specimen, the same micro-segregation was observed in the AP and H1150 specimen.

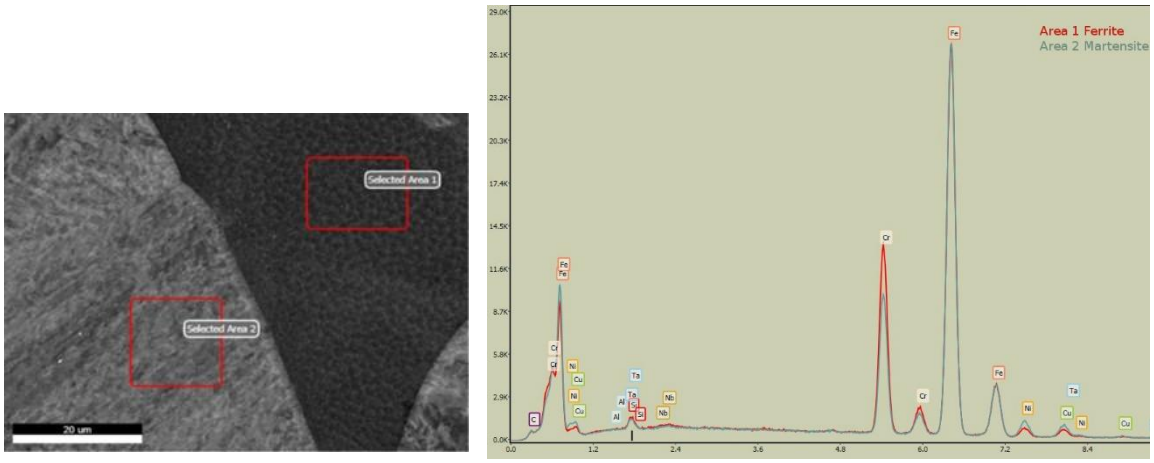

Figure 23 EDS analysis of the two generall phases in the microstructure of H900 specimen.

The as-printed micrographs shown in Figure 9A&B revealed the presence of large particles in the δ-ferrite matrix. The particles were visible in both LOM and BSE. The particles appeared bright in the BSE micrograph, indicating the presence of heavier elements than the surrounding matrix. EDS analysis, shown in Figure 10, helped reveal that these particles were in fact rich in either copper or niobium.

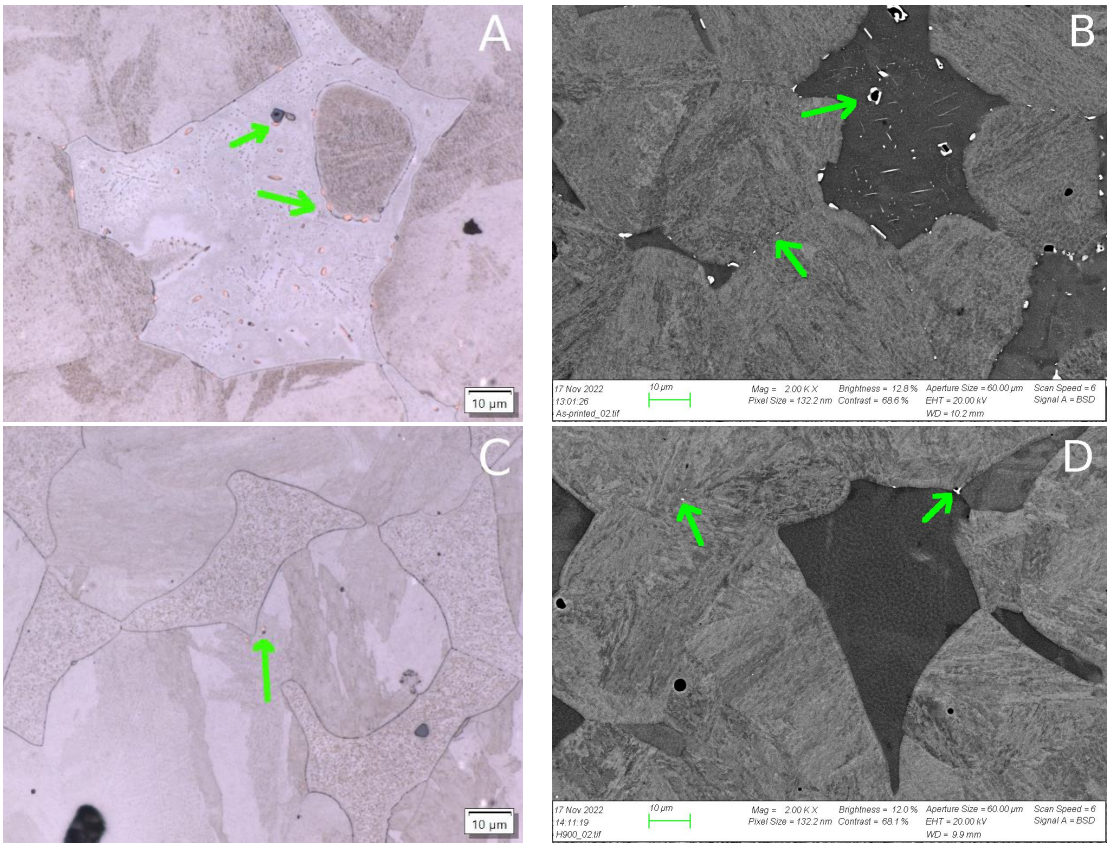

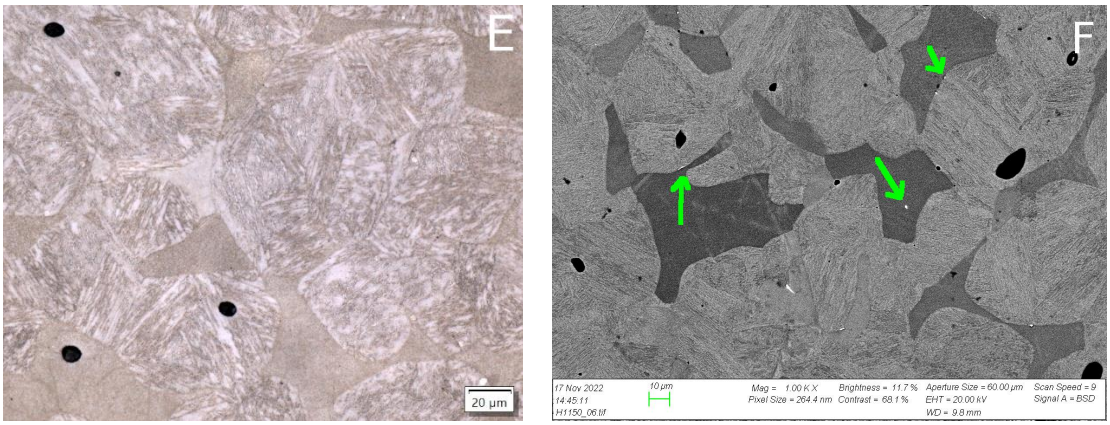

Figure 24 LOM and BSE micrographs. A and B are AP, C and D are H900, and E and F is H1150. Green arrows point to particles. LOM images are etched using Fry's reagent.

These particles are the remnants of the sintering process. It is established that densification often manifests more predominantly in the δ-ferrite matrix [26]. Low solubility of FCC copper and niobium carbide in δ-ferrite, and the fact that the rate of self diffusion is higher in δ-ferrite [17, p. 190] are reasons that they form particles at pores and grain boundaries. Even after the pore has been filled, the particles can remain [26].

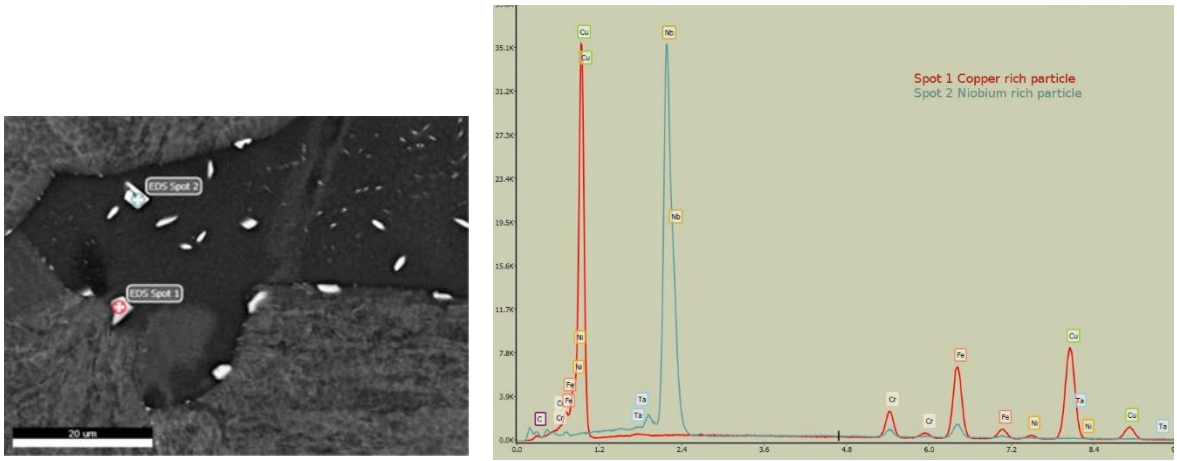

Figure 25 EDS analysis of the particles. It was found that the particles were either rich in Niobium or Copper

Figure 9C&D show the microstructure after solution treatment and H900 aging. The matrix δ-ferrite is mostly cleared of large particles. Particles are still found however at the δ-α' grain boundaries and adjacent to pores. Solution treatment has allowed for particles to disperse as found by Li et al [27], longer soaking times would lead to the dissipation of the remaining particles.

The same particles seem to remain after H1150 aging, as shown in Figure 9E&F, suggesting that the aging temperature is to low to allow for diffusion to take place. Although the microstructure looks similar in the BSE, the LOM micrographs show that the α' phase has undergone some change. It is also interesting to note that the etchant seemed to attack the H1150 surface more aggressively than that of the As-printed and H900.

4.5 Fractography

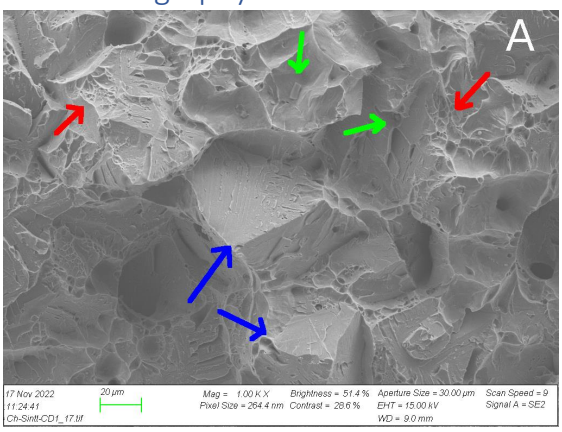

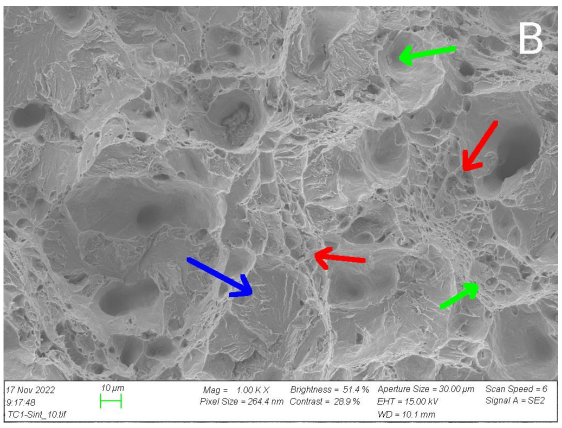

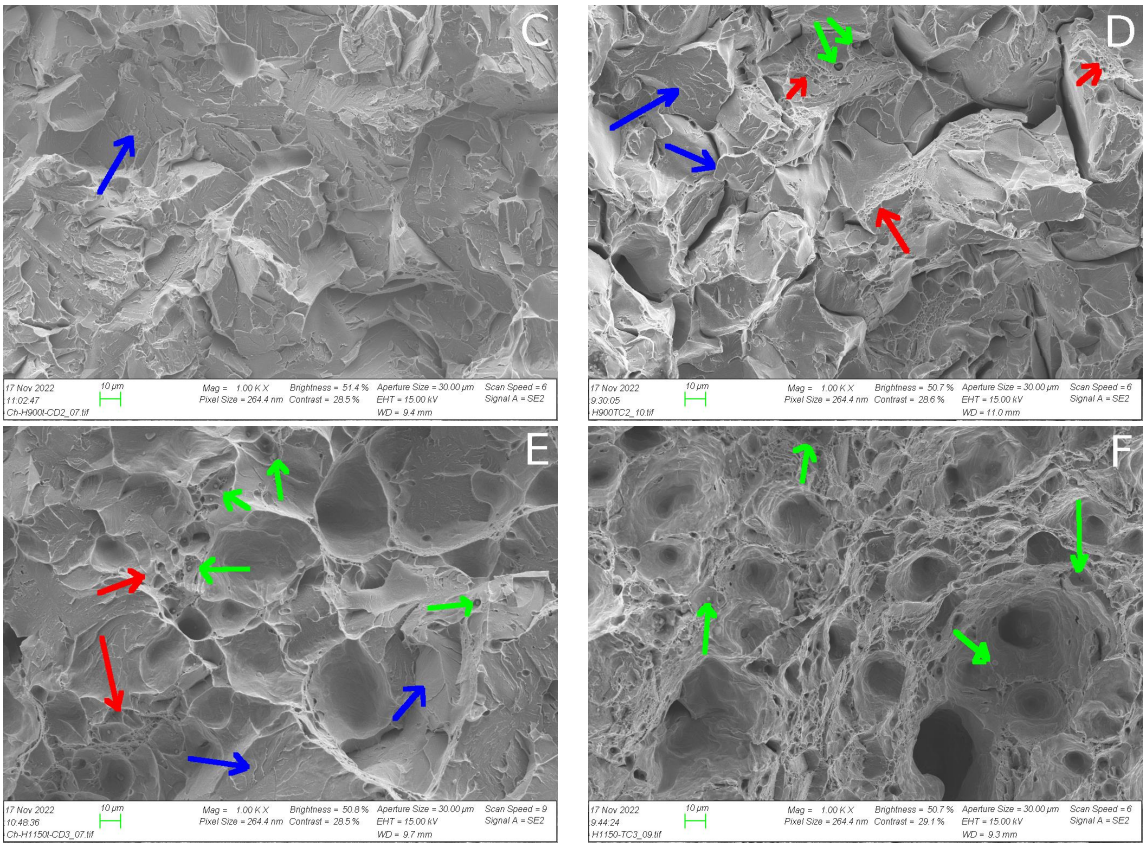

Figure 26 Fracture surface captured with SEM. A is CVN AP, B is tensile AP, C is CVN H900. D is tensile H900, E is CVN H1150 and F is tensile H1150. Blue arrows point to transgranular cleavage planes, red arrows point to dimples and green arrows point to inclusions.

The fracture surfaces display a variety different fracture characteristics. It is important to remember that the morphology is also a result from the rate of straining induced in the two fracture methods. In Figure 26A,C&E are the CVN specimen. The AP specimen in Figure 26A shows a mixed fracture surface. Thin bands of dimples seems to suggest the presence of intergranular fracture. There is also observed a fair amount of large inclusions, some of them with irregular shapes. They are observed on surfaces that resemble grain boundaries, suggesting that they facilitate intergranular fracture. Some cleavage planes are also present showing river patterns.

In the H900 specimen in Figure 26C, only signs of brittle fracture is present mostly transgranular cleavage planes with river patterns. In the H1150 specimen ,Figure 26E the surface shows a more ductile character. The presence of large dimples suggest fracture by microvoid coalescence. Thin bands of dimples are also present, some with inclusions visible. There are also some transgranular cleavage planes visible.

In the tensile specimens in Figure 26B,D&E ductile, fracture is more apparent, this is to be expected as the strain rate is lower. The AP specimen in Figure 26B there are faces showing cleavage fracture, surrounded bands of dimples. Many of the dimples have inclusions inside. The H900 specimen in Figure 26D shows mostly characteristics of cleavage fracture. Thin bands of dimples and the fact that the shape of the grains seem to be apparent suggest that a large portion of the fracture mechanism is intergranular cleavage. There is also an amount of transgranular planes visible. Figure 26E shows the fracture surface of the H1150 specimen. The structure is predominantly consisting of dimples, it suggests that the fracture mode was a ductile in nature.

5 Discussion

The main objective of this thesis is to understand the mechanical properties of the specimen. It is helpful to compare with other findings.

5.1 Comparison with MIM

The BJP shares some similarities with MIM in the sense that both rely on sintering a powder, and densification through pore shrinkage to achieve desired mechanical properties. MPIF has provided a standard which clarifies nomenclature around MIM, additionally it also lists values for mechanical properties for various metal alloys commonly used in MIM. Both minimum and typical values for 17-4 PH MIM can be found in the MPIF standard 35-MIM [28, p. 13]

Typical values from MPIF 35 MIM are listed along with rounded values obtained in this thesis from table 7.

*Table * Converted from HRC to HV using conversion table [29, p. 550]*

Condition	As printed	MIM-sintered	H900	MIM-H900
Yield [MPa]	788	730	1162	1090
UTS [MPa]	917	900	1302	1185
Elongation [%]	5.5 in 50mm	6 in 25 mm	7.5 in 50mm	6 in 25mm
Hardness	304.0	279*	416.2	327*

5.2 Comparison with recent study

In a recent study by Radhakrishnan et al [15] , BJP was used to print samples of 17-4 PH. The two batches represent different parameters in the sintering stage. Batch B was found to have fewer pores, compared to Batch A.

The tensile specimen in their study, was of the flat dog bone shape. The gauge length used was 20 mm. Comparison between this thesis and the report is therefore strictly not valid, as the specimen are very different in geometry.

The mechanical properties seem to agree, except for the elongation behavior reported for Batch A. The low amount of elongation in Batch A H1150 is attributed to the amount of pores present. Why elongation seemed to decrease from H900 to H1150 is not clear.

Rounded values are compared with values from the study. Although not strictly compatible, it is interesting to compare.

Condition: H900	This thesis	Batch A	Batch B
Yield [MPa]	1162	1079	1057
UTS [MPa]	1302	1294	1321
Elongation [%]	7.5	8.3	7.4

Condition: H1150	This thesis	Batch A	Batch B
Yield [MPa]	707	760	738
UTS [MPa]	918	1001	960
Elongation [%]	12.8	5.6	15.9

The samples in the study were allowed to soak in the solution treatment for two hours. This allows for more diffusion in the γ-phase region, reducing the amount of δ-ferrite. The remaining microstructure has lower amounts of retained δ-ferrite, improving mechanical properties.

5.3 Hardness testing of the x-axis could be affected by work hardening.

Upon later reflection it was recognized that the hardness measurements from the x-planes might be slightly off because yielding in the material could have propagated further out in the sample. The fracture end was cut off to be used for analysis in the SEM machine, approximately 1 cm in length. Yielding could likely occur at least 1 cm out from the fracture end. The degree of plastic deformation in the samples seemed to be low, but the possibility that strain hardening could have manifested at locations where hardness testing was conducted is possible. In hindsight, it was a mistake to conduct hardness testing on these pieces.

5.4 Toughness

It was interesting to see how the heat treatments resulted in varying forms of toughness.

The AP specimen show the post sintering microstructure. It can be imagined that the large particles work as nucleation points for voids. This is observed on Figure 26 A&B. Both CVN and tensile fracture surfaces display dimples, often with inclusions. The large particles also seem to facilitate some degree of intergranular fraction. They often manifest heavily on grain boundaries, as seen on Figure 24 A&B ,resulting in a weak cohesion between grains. Some cleavage planes are also visible.

High strength is achieved in the H900 samples, as shown in Figure 21. This could correlate with the fact that the large particles have mostly been dissolved as shown in Figure 24 C&D . Additionally, the H900 aging has allowed for precipitation of fine coherent particles that impede dislocation movement. The dislocation buildup in the δ -ferrite because of the martensite transformation is still present. Looking at the fracture surface of the tensile specimen Figure 26 D, it seems that a lot of the fracture has propagated along the grain boundaries. Small bands of dimples are also observed. This could suggest that the material has separated at the grains, the δ-ferrite in between plastically deforming. This amounts to a higher stress and strain combination than that of the AP sample. However, looking at the CVN sample Figure 26 C, shows how the fracture is primarily consisting of transgranular cleavage planes. The crack has propagated through the grains in unstable fashion. Essentially the material is too stiff to allow crack fronts to deform, so critical stress is achieved. The low fracture toughness of the material is concerning regarding the fact that the material has pores.

As the discussed earlier, aging beyond H900 results in increased ductility at the expense of strength. This was also the case in this thesis. H1150 showed the greatest toughness and CVN of the samples. The reason for this is thought to be increased recovery the strained δ-ferrite regions, tempering of the martensite, the coarsening of copper precipitates and the formation of austenite in lath boundaries. The H1150 also shows signs of strain hardening, as shown in Figure 21.

5.5 Particles

The As-printed samples contained large particles of copper and niobium-carbide. These particles seemed to become less prevalent and smaller in size after ageing. It was clearly observable that these particles seemed to propagate in the ferrite matrix and around pores, but they were most abundant in the grain boundaries. These particles are the remnants from the sintering process. It plausible that longer soaking time in the solution treatment process, would dissolve more of the particles and allow the γ-phase to grow in size. This should bring about superior mechanical properties, as the hardening mechanism in PH steels propagates primarily in the martensite region.

The particles seen in this thesis seemed to have a detrimental effect on the mechanical properties. It is possible that they induce different fracture modes in the material. Incoherent particles are good nucleation points for microvoid, also it seems that since these particles tend to manifest at grain boundaries that they can weaken the coherency between grains. Inducing intergranular fracture.

5.6 CVN specimen ligament

Table 1 in the appendix show raw data for CVN. One parameter that was recorded was the ligament. The ligament in the specimen is the material from the pint of the notch to the opposite side. It is the remaining material after the notch is cut. The tolerance as specified in the standard is +/- 0.075 mm. Before the testing took place, this was measured using callipers. It was found that two samples were out of tolerance. However, no abnormal values were observed in the testing. It is likely that since all the samples are very brittle, that this error does not manifest itself very profoundly. It is never the less a discrepancy from the standard.

6 Conclusion

The objective of the thesis was to investigate the microstructure and mechanical properties of 17-4 PH samples made through BJP. As was expected with a PH alloy, the mechanical properties can be controlled to a certain degree by aging the material. As with conventional 17-4PH the H900 aging regime leads to peak hardness, however the material is brittle and has weak notch toughness. Over aging induces some ductile behavior at the expense of hardness. The mechanisms for this has to do with copper particles in the martensite phase. H900 allows for fine coherent particles in the martensite, the martensite also induces strain upon the δ-ferrite inhibiting dislocation motion. Over-aging leads to recovery in the δ-ferrite and larger precipitates of copper in the martensite. They may loose coherency t at this stage, allowing for easier dislocation movement. The copper may also induce development of austenite at the lath boundaries.

The microstructure of 17-4 PH can take on many forms as a function of the AM technology being used. The sintering process that ultimately fuses the particles together and become solid through densification. The mechanism that allows for this to happen successfully in BJP is the development of δ-ferrite that happens at sintering temperature. δ-ferrite nucleate at the particle boundaries, and through diffusion gradually cohere the particles together. Upon cooling, a portion of δ-ferrite is converted back into γ austenite then α'martensite . It is desirable that the final structure has as much martensite as possible, since this is the phase where age hardening mainly propagates.

When sintering is completed, it is advantageous to soak the material in the γ-phase region. In this thesis, 0,5 hour was used in the solution treatment, large amounts of retained δ-ferrite was observed. Extending this time will likely help dissolve large particles in the δ-ferrite and expand γ-phase. Parts created from JBP, require longer periods of solution treatment than that of conventionally produced 17-4 PH. Maybe using nitrogen gas in the solution treatment phase would accelerate this process, this would be something to look at in future work.

Hardness measurements were conducted in all three axis in relation axis of build bed. Similar values suggests a isotropic material. It was also observed that the surface of the H1150 sample seemed to be more susceptible to the etching, suggesting that corrosion properties may affected by aging time.

Reference

[1] ISO/ASTM, “Additive manufacturing- General principles - Fundemantals and vocabulary,” ISO/ASTM International, 2021.

[2] M. P. Groover, Fundamentals of modern manufacturing, 7th ed., Singapore: Wiley, 2021.

[3] Sintef, “Additive manufacturing (3D printing),” 2022. [Online]. Available: https://www.sintef.no/en/sintef-research-areas/additive-manufacturing-3d-printing/. [Accessed 15 12 2022].

[4] H. Lipson and M. Kurman, Fabricated: The new world of 3d printing, Willey, 2013.

[5] ASM, ASM speciality handbook, Stainless steel, 1999.

[6] h. k. bhadeshia and r. w. honeycombe, Steels, 4th ed., cambridge: elsevier, 2017.

[7] G. E. Totten, Steel Heat Treatment, 2 ed., taylor & francis group, 2007.

[8] Desktop metals, “17-4 ph stainless steel material data sheet,” [Online]. Available: https://www.desktopmetal.com/uploads/SHP-SPC-MDS_17-4PH-220427.pdf. [Accessed september 2022].

[9] Outokumpu High Performance Stainless, “Type 630, 17 Cr-4Ni UNS 17400,” Bannockburn IL. USA, 2022.

[10] X. Ma, Z. Wang, X. Tong, X. Du, T. Li, R. Liu, Y. Liu and D. Cheng, “SPINODAL DECOMPOSITION OF PRECIPITATION HARDENING,” *Materials and technology,* vol. 2, pp. 193-199, 2022.

[11] S. Banerjee, R. Krishnan and U. Viswanathan, “Effects of aging on the microstructure of 17-4 PH stainless steeel,” *Materials science and engineering,* pp. 181-189, 1988.

[12] Y. Wu, D. Blaine, B. Marx, C. Schlaefer and R. German, “Sintering Densification and Microstructural Evolution of,” *Metallurgical and materials transactions,* vol. 33a, july 2002.

[13] Y. WU, R. M. GERMAN, D. BLAINE, B. MARX and C. SCHLAEFER, “Effects of residual carbon content on sintering shrinkage, microstructure and mechanical properties of injection molded 17-4 PH stainless steel,” 2002.

[14] ASTM International, “A693-16 Standard specification for Precipiytation-hardening and heat-resisting Steel plate,sheet and strip,” ASTM, 2022.

[15] J. Radhakrishnan, P. Kumar, S. S. Gan, A. Bryl, J. McKinnell and U. Ramamurty, “Microstructure and tensile properties of binder jet printed 17-4 PH martensistic stainless steel,” *Materials science and engineering,* vol. 860, 2022.

[16] C. Hsiao, C. Chiou and J. Yang, “Aging reactions in a 17-4 PH stainless steel,” *Materials Chemistry an physics,* vol. 74, pp. 134-142, 2002.

[17] w. Callister and D. Rethwisch, Material Science and engineering, 9 ed.

[18] ASM, Metals handbook vol. 9 Metallography and microstructures, 9th ed., vol. 9, Metals park, Ohio, 1992.

[19] ASM, Metals handbook vol. 9 Fractography and atlas of fractographs, Metals park, Ohio, 1974.

[20] O. K. Bjørge, “Mechanical properties of 316L stainless steel made by selective laser melting using powder produced from recycled scrap material by vacuum induction gas atomizing,” stavanger, 2021.

[21] DNV, “DNV-ST-B203 Additive manufacturing of metallic parts,” 2021.

[22] «Metalliske materialer Charpy-skårslagprøving Del1 ISO 148-1:2016,» Norsk Standard, 2016.

[23] ASTM, “E8/E8M Standard test methods for tension testing of metallic materials,” 2022.

[24] ASTM, “Standard practice for microetching metals and alloys E407,” ASTM, 1999.

[25] ISO, “ISO 6507-1 Metallic materials Vickers hardness test part 1: tet method,” Iso, 2018.

[26] A. D. Akessa, W. M. Tucho, G. H. Lemu and J. Grønsrud, “Investigations of the Microstructure and Mechanical Properties,” MDPI, Stavanger, 2022.

[27] K. Li, S. Sridar, S. Tan and W. Xiong, “Effect of homogenization on precipitation behaviour and strengthening of 17-4 PH stainless steel fabricated using laser powder bed fusion,” Pittsburg, 2021.

[28] MPIF, “MPIF 35 MIM Materials Standards for Metal Injection Molded Parts,” MPIF, New Jersey, 2018.

[29] ASM, Metals handbook vol. 8 Mechanical testing and evaluation, Metals park, Ohio, 2000.

[30] Y. W. C. S. B. M. a. R. G. D.C. Blaine*, Sintering Shrinkage and Microstructure Evolution during Densification of a Martensic steel, Pennsylvania State University, 2003.

[31] C. R.Simcoe, “The discovery of strong aluminium,” *ADVANCED MATERIALS & PROCESSES,* pp. 35-36, august 20211.

[32] ASTM, “B 883 Standard specification for metal injection molding (MIM) Ferrous materials,” ASTM, 2005.

[33] D. Pugliesi, *Phase diagram of pure iron,* 2010.

Appendix

Charpy data

Table 1

Navn	Condition	Ligament [mm]	Digital [J]	Analog [J]
AB_1	AP	8.05	8.3	10.3
BD_1	AP	8.05	7.8	9.8
CD_1	AP	8.05	7.5	9.5
AB_2	H900	7.80	2.3	4.3
BD_2	H900	8.00	2.3	4.3
CD_2	H900	8.00	2.6	4.6
AB_3	H1150	8.05	28.0	30.0

BD_3	H1150	7.85	28.1	30.1
CD_3	H1150	8.05	29.8	31.8

Hardness data

Table 2

	As printed			H900			H1150		
	x	y	z	x	y	z	x	y	z
1	313.3	300.2	320.7	403.7	429.8	421.7	289.9	286.7	287.4
2	313.7	305.0	313.1	408.2	431.0	417.5	288.3	289.1	287.0
3	312.9	302.8	309.3	404.7	414.3	411.8	293	291.2	286.8
4	306.2	310.9	311.7	411.4	404.0	427.9	293.5	286.5	292.6
5	311.6	307.1	302.4	413.9	420.2	412.4	291.4	289	283.0
6	307.8	302.5	302.1	401.1	430.3	437.2	293.2	288.5	294.4
7	307.1	293.8	293.7	422.4	421.2	416.7	283.7	292.6	290.3
8	306.8	297.6	301.6	418.8	421.7	423.2	293.1	294.4	289.3
9	315.0	308.7	294.3	406.6	408.2	415.3	288.7	291.7	292.7
10	298.6	298.6	295.3	413.1	410.7	407.9	292.3	296.2	294.4
11	297.3	308.2	285.8	420.4	425.7	414.8	290.9	300.9	292.0
12	298.2	302.9	298.7	418.0	417.8	401.1	291.9	301.5	292.9
13	304.0	306.8	289.5	414.7	414.5	416.1	306	292.7	300.7
Avg	**307.1**	**303.5**	**301.4**	**412.1**	**419.2**	**417.2**	**291**	**292.4**	**291**
SD	**5.93**	**4.79**	**9.68**	**6.56**	**8.33**	**8.67**	**4.82**	**4.66**	**4.31**

Tensile data

lørdag 26. november 2022

Instron Applications Laboratory

Martin og Stian Bacheloroppgave Høst 2022
PH17-4 persipitatherdbart stål
ASTM E8-11 - Standard test method for tension testing of metallic materials.

Operator ID	
Company	
Required number of specimens in prompted test sample	1
Control mode 1	Strain rate [Adaptive]
Rate 1	0,015 mm/mm/min
Control mode 2	Estimated strain rate
Rate 2	0,100 mm/mm/min
Changeover (1 to 2)	Yield (Offset 0.2 %)

Metals Tensile - Specimen 1 to 3

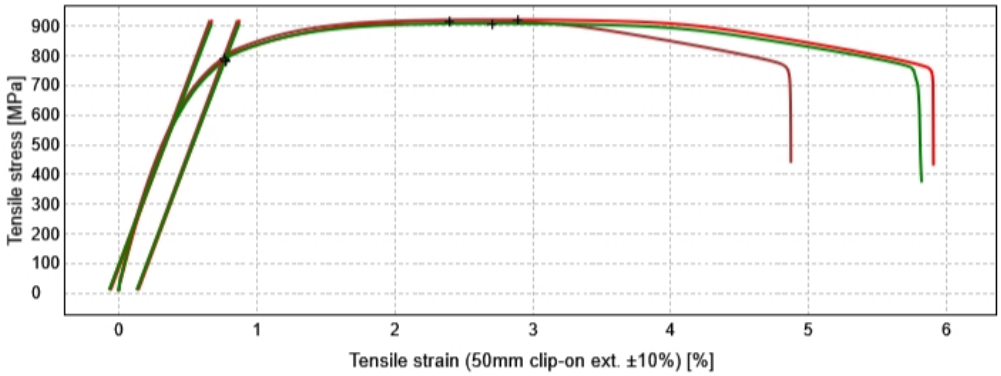

	Specimen label	Modulus (E-modulus) [GPa]	Tensile stress at Tensile strength [MPa]	Tensile strain (50mm clip-on ext. ±10%) at Break (Standard) [%]	Strain hardening exponent at n-value (Automatic)	50mm clip-on ext. ±10% gauge length [mm]	Tensile strain (50mm clip-on ext. ±10%) gauge length [mm]	Varmebehandling	Tensile stress at Yield (Offset 0.2 %) [MPa]
1	T_A_1	123,76	921,091	5,887	0,12	50,00	50,00	Sintra	790,04
2	T_B_1	124,65	920,070	4,854	0,13	50,00	50,00	Sintra	791,79
3	T_C_1	120,98	909,095	5,801	0,12	50,00	50,00	Sintra	782,35
Mean		123,13	916,752	5,514	0,12	50,00	50,00	-----	788,06
SD		1,9122	6,651	0,573	0,0069	0,0000	0,0000	-----	5,0230
COV		1,5530	0,725	10,397	5,5406	0,0000	0,0000	-----	0,6374

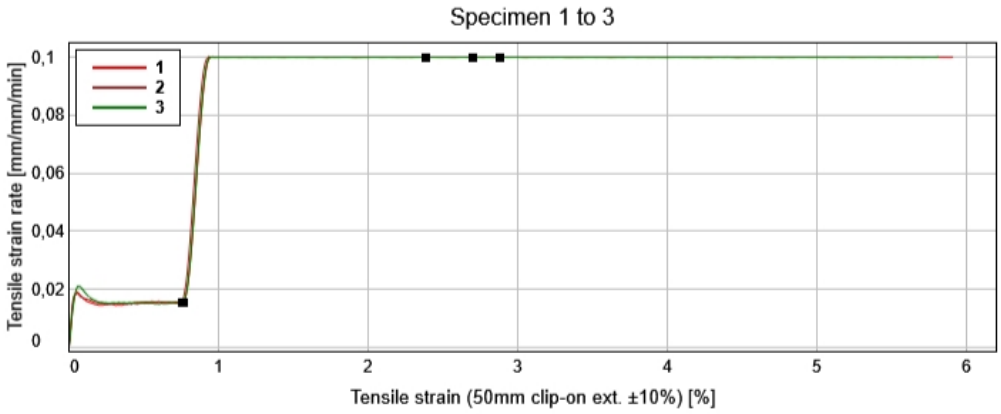
Specimen 1 to 3
1
2
3
Tensile strain rate [mm/mm/min]
0,1
0,08
0,06
0,04
0,02
0
0
1
2
3
4
5
6
Tensile strain (50mm clip-on ext. ±10%) [%]

lørdag 26. november 2022

Instron Applications Laboratory

Martin og Stian Bacheloroppgave Høst 2022
PH17-4 persipitatherdbart stål
ASTM E8-11 - Standard test method for tension testing of metallic materials.

Operator ID	
Company	
Required number of specimens in prompted test sample	1
Control mode 1	Strain rate [Adaptive]
Rate 1	0,015 mm/mm/min
Control mode 2	Estimated strain rate
Rate 2	0,100 mm/mm/min
Changeover (1 to 2)	Yield (Offset 0.2 %)

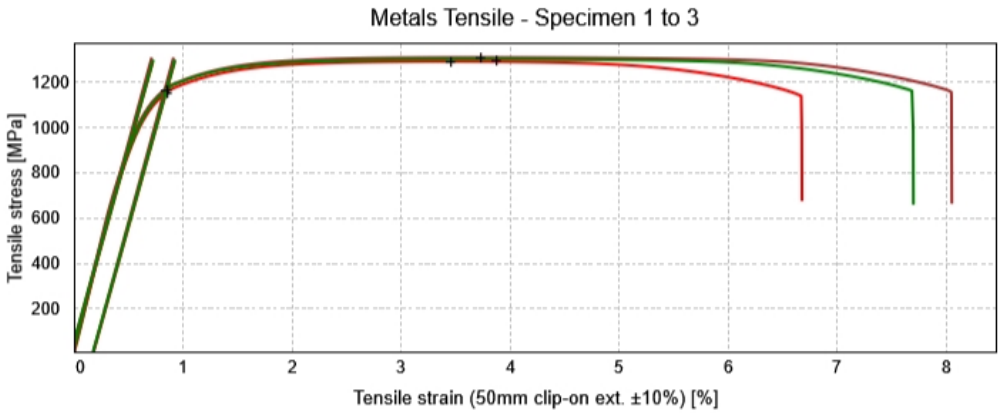

	Specimen label	Modulus (E-modulus) [GPa]	Tensile stress at Tensile strength [MPa]	Tensile strain (50mm clip-on ext. ±10%) at Break (Standard) [%]	Strain hardening exponent at n-value (Automatic)	50mm clip-on ext. ±10% gauge length [mm]	Tensile strain (50mm clip-on ext. ±10%) gauge length [mm]	Varmebehandling	Tensile stress at Yield (Offset 0.2 %) [MPa]
1	T_A_2	172,36	1292,330	6,659	0,09	50,00	50,00	H900	1152,60
2	T_B_2	176,25	1310,176	8,032	0,08	50,00	50,00	H900	1168,61
3	T_C_2	172,00	1301,965	7,681	0,08	50,00	50,00	H900	1165,61

	Specimen label	Modulus (E-modulus) [GPa]	Tensile stress at Tensile strength [MPa]	Tensile strain (50mm clip-on ext. ±10%) at Break (Standard) [%]	Strain hardening exponent at n-value (Automatic)	50mm clip-on ext. ±10% gauge length [mm]	Tensile strain (50mm clip-on ext. ±10%) gauge length [mm]	Varmebehandling	Tensile stress at Yield (Offset 0.2 %) [MPa]
Mean		173,54	1301,490	7,457	0,08	50,00	50,00	-----	1162,28
SD		2,3573	8,933	0,713	0,0049	0,0000	0,0000	-----	8,5098
COV		1,3584	0,686	9,566	6,0488	0,0000	0,0000	-----	0,7322

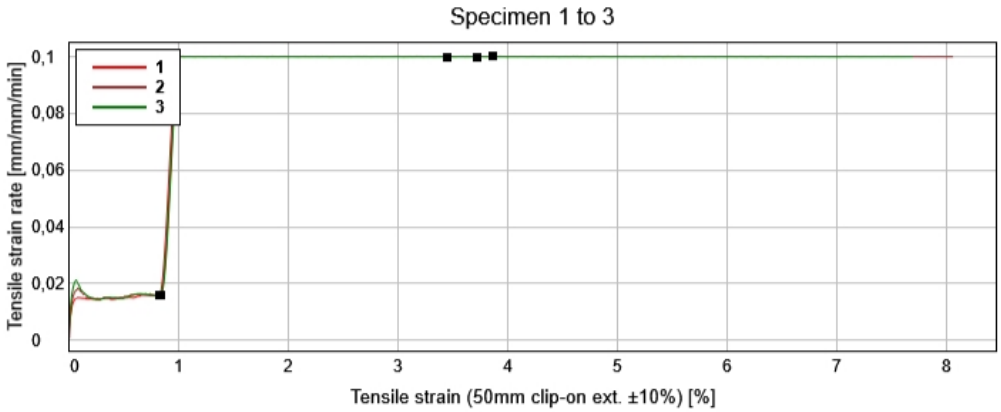

lørdag 26. november 2022

Instron Applications Laboratory

Martin og Stian Bacheloroppgave Høst 2022
PH17-4 persipitatherdbart stål
ASTM E8-11 - Standard test method for tension testing of metallic materials.

Operator ID	
Company	
Required number of specimens in prompted test sample	1
Control mode 1	Strain rate [Adaptive]
Rate 1	0,015 mm/mm/min
Control mode 2	Estimated strain rate
Rate 2	0,100 mm/mm/min
Changeover (1 to 2)	Yield (Offset 0.2 %)

Metals Tensile - Specimen 1 to 3

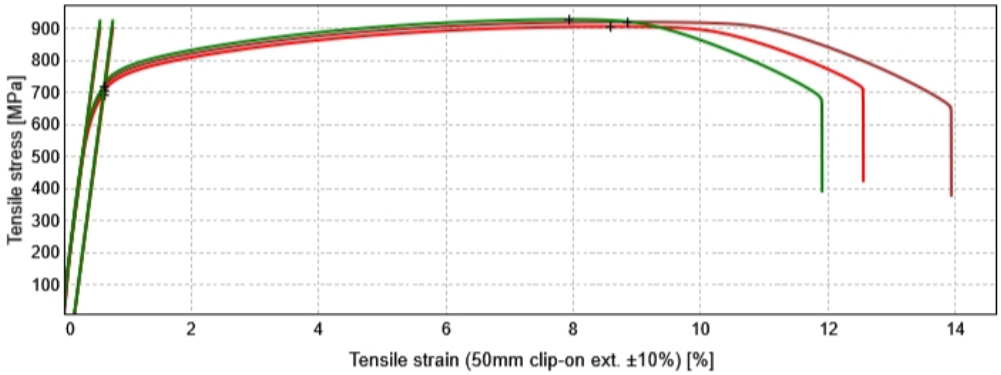

	Specimen label	Modulus (E-modulus) [GPa]	Tensile stress at Tensile strength [MPa]	Tensile strain (50mm clip-on ext. ±10%) at Break (Standard) [%]	Strain hardening exponent at n-value (Automatic)	50mm clip-on ext. ±10% gauge length [mm]	Tensile strain (50mm clip-on ext. ±10%) gauge length [mm]	Varmebehandling	Tensile stress at Yield (Offset 0.2 %) [MPa]
1	T_A_3	148,42	905,278	12,541	0,12	50,00	50,00	H1150	694,61
2	T_B_3	150,77	919,485	13,922	0,12	50,00	50,00	H1150	706,82
3	T_C_3	151,64	927,668	11,893	0,12	50,00	50,00	H1150	719,33
Mean		150,28	917,477	12,785	0,12	50,00	50,00	-----	706,92
SD		1,6660	11,330	1,036	0,0006	0,0000	0,0000	-----	12,3611
COV		1,1086	1,235	8,106	0,4686	0,0000	0,0000	-----	1,7486

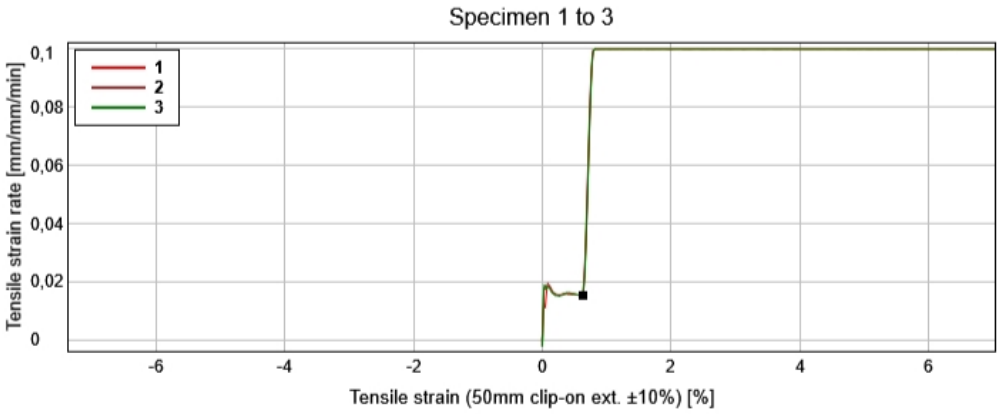
Specimen 1 to 3
1
2
3
Tensile strain rate [mm/mm/min]
0,1
0,08
0,06
0,04
0,02
0
-6
-4
-2
0
2
4
6
Tensile strain (50mm clip-on ext. ±10%) [%]